OBSERVATIONS OF ENERGETIC ELECTRONS ($E \geqslant 200$ keV) IN THE EARTH'S MAGNETOTAIL:

PLASMA SHEET AND FIREBALL OBSERVATIONS

D. N. Baker and E. C. Stone

California Institute of Technology
Pasadena, California 91125

October 1976

SRL 76-3

A B S T R A C T

Using the Caltech Electron/Isotope Spectrometer (EIS) aboard the earth-orbiting spacecraft IMP-8, intense energetic electron events ($E \geqslant 200$ keV) have been observed at $\sim 30\ R_E$ in the magnetotail on 13 of 28 magnetotail passes. In one class of events, peak absolute intensities $j(E \geqslant 200\ \text{keV}) = 10^3 - 10^4$ electrons $(\text{cm}^2\text{-sec-sr})^{-1}$ are detected; the differential energy spectra for these events are very steep, with power-law indices ~ 7. For this class of observation, symmetric electron pitch angle distributions are detected with the presence of little or no unidirectional streaming, consistent with quasi-trapped motion of the particles. Concurrent observations with other instrumentation on the same spacecraft indicate that the local magnetic fields possess northward components while simultaneous plasma ($50\ \text{eV} \leq E \leq 45\ \text{keV}$) data show bulk flow speeds of a few hundred km sec^{-1} or less, with intense plasma heating ordinarily occurring. A second distinct class of events corresponds to lower average absolute electron intensities ($E \geqslant 200$ keV), typically harder electron energy spectra, and strong, intermittent field-aligned (and tailward) unidirectional streaming of the energetic electrons. During periods when the latter class of events are observed in the plasma sheet, strong southward components are found in the local magnetic fields and large tailward bulk plasma flow has been reported (with tailward jetting in excess of 1000 km sec^{-1} in certain cases). The second class of events is consistent with energetic electron motion on essentially open field lines. These streaming events are found to be associated with apparent localized acceleration regions in the magnetotail.

INTRODUCTION

Energetic electron intensities at large geocentric distances in the earth's magnetotail have been studied extensively during the last decade (Anderson, 1965; Montgomery et al., 1965; Bame et al., 1967; Montgomery, 1968; Haskell, 1969; Retzler and Simpson, 1969; Singer and Bame, 1970; Meng, 1971). In a prior report (Baker and Stone, 1976), we have briefly summarized the results of these previous papers in which the observations were ordinarily presented for electron energy thresholds $E \sim 40$ keV, often with relatively high flux detection thresholds.

Recently, the earth-orbiting IMP-7 and IMP-8 spacecrafts have afforded a further opportunity to simultaneously study the properties of plasma waves and particles, the local magnetic fields, and the very energetic particle component in the magnetotail. IMP-8 (launched October 1973) has an orbital period of ~ 12 days and spends roughly 3 days within the magnetotail during each orbit. The nominal orbital parameters (perigee $\sim 23\ R_E$, apogee $\sim 46\ R_E$, and inclination $\sim 29^o$) make IMP-8 well suited for providing broad coverage of the cislunar magnetotail. IMP-7 has a similar, though somewhat more circular, orbit.

Sarris et al.(1976) have reported IMP-7 data showing unidirectional streaming of protons ($E_p > 0.29$ MeV) and electrons ($E_e > 0.22$ MeV) in the magnetosheath with flow in the tailward direction. Within the magnetotail, Sarris et al. have found highly anisotropic proton bursts but these authors have concluded that energetic electrons are mainly isotropic throughout the magnetotail.

Frank et al. (1976) have reported on the plasmas, the magnetic fields, and the energetic electron ($E_e > 45$ keV) properties at $\sim 30\ R_E$ as seen with

IMP-8 during 1974. Using the concurrent body of 1974 data for the Caltech EIS, we have studied results for electrons $\gtrsim$ 200 keV. In Baker and Stone (1976) we briefly described some of the energetic electron anisotropies observed in conjunction with the acceleration regions identified by Frank et al. (1976). In the present paper we give more detailed analyses of our observations in the distant plasma sheet including specific features of intensities, energy spectra and pitch angle distributions of the very energetic electrons associated with intense plasma particle events (50 eV $\leq$ E $\leq$ 45 keV) detected with University of Iowa electrostatic analyzers. In a companion paper we report on observations in the magnetotail boundary layer.

INSTRUMENTATION

The Caltech Electron/Isotope Spectrometer (EIS) aboard IMP-8 is schematically illustrated in Figure 1. The telescope comprises a stack of eleven totally depleted surface-barrier solid-state detectors surrounded by a plastic scintillator anticoincidence cup. One of the solid-state detectors (D2) is 47 μm thick, while all other detectors in the stack are 1 mm thick. In addition, the first two detectors in the telescope (D0 and D1) are annular and provide active collimation for a detection mode termed "narrow geometry". Protons and other nuclei are counted with high efficiency in D2 while electrons are not. Hence a clean separation of electrons from protons is possible in narrow geometry by requiring the triggering of detector D5 in coincidence with D2 (for protons) or in anticoincidence with D2 (for electrons).

In this paper we shall make primary use of counting rates from an instrument mode termed "wide geometry". This particular mode consists of

count rates from particles which pass through the thin (~ 3.2 mg cm^{-2}) mylar window of the telescope, trigger detector D0, and then stop in the stack before triggering D10 or D11. Although both electrons and protons are counted in this mode, we use it because of its large geometric factor and, hence, improved counting statistics. Using the other simultaneous detection capabilities of the narrow geometry, it has been determined that protons ordinarily make a relatively minor contribution to the counting rates presented here.

The EIS instrument also has a neutral analysis mode which requires the triggering of D7 without triggering D0, D1, D3, D4, D5, D10, or D11. This mode is used to monitor the background due to the neutral radiation component such as gamma rays and neutrons which interact in the detector stack after being generated by the nuclear interaction of high-energy cosmic rays in the spacecraft.

For the absolute electron intensities presented in this paper we have used the neutral analysis and narrow geometry detection modes of the EIS to subtract the proton, neutral, and cosmic ray nuclei contributions to the wide geometry counting rates. The response properties of relevance for this study are summarized in Table 1. Additional details about the EIS and its response properties are given by Hurford et al. (1974) and Mewaldt et al. (1976).

It is found that the energy spectra of electrons in the plasma sheet are fairly steep (commonly having differential power law indices $\gtrsim 3$). It is seen in Table 1 that the D0* and D01* counting rates have passbands with effective upper cutoffs at $E_e \sim 6$ MeV. Because of the steep electron spectra observed, we shall regard the background-corrected D0* and D01 counting rates

as being proportional to the integral intensities of electrons above the threshold energies of Table 1. These integral intensities will subsequently be labeled as the $E \geqslant 200$ keV fluxes and the $E \geqslant 1$ MeV fluxes, respectively.

The EIS also provides concurrent pulse height analysis data from which the detailed differential energy spectra for electron energies $E \geqslant 160$ keV may be determined. The pulse height analysis (PHA) data used subsequently in this paper are obtained in the narrow geometry detection mode. Events are analyzed in detector D5 with the requirement that the particle not have triggered D2. This detector combination allows very clean separation of electrons and nuclei. The individual pulse-height analyzer channel widths in D5 are ~ 40 keV, which represents the maximum energy resolution available with the Caltech experiment. We ordinarily use the first 50 PHA channels of D5 and hence extend our event analysis to ~ 2 MeV.

Of particular note is the high degree of insensitivity of the PHA data to electron pile-up. For conditions of high intensities and steep energy spectra, it is possible for count rates in thick detectors to be due to two or three-fold coincidences of stopping electrons of energy well below the normal detection threshold. In the EIS instrument, the 47 μm detector D2 is present in front of the thick detector (D5) in which the electron pulse height analysis is performed and D2 acts to stop electrons $E \leqslant 90$ keV. Hence, the PHA data are not contaminated by very high intensities of these low-energy electrons.

Angular distributions may be studied in all of the detection modes described above. The IMP-8 spacecraft rotates about an axis very nearly perpendicular to the ecliptic plane, with a spin period of ~ 2.6 seconds.

The angular distributions to be discussed here will be primarily for electrons $E \geqslant 200$ keV. The counts in this channel are accumulated in eight sun-fixed 45° sectors by an onboard system. Each sample represents an accumulation for 7 consecutive spacecraft rotations (i.e., ~ 20 seconds) and the 20-second sample is then read out once every 81.92 seconds. All angular distributions described herein are established within this eight-sector framework. We label each angular distribution by the nearest second UT to the start of the accumulation period.

The range of pitch angles sampled in each rotation depends upon the cone angle Γ between the magnetic field vector and the spacecraft spin vector. If the local magnetic field vector is perpendicular to the spin vector ($\Gamma = 90^{\circ}$), then in each rotation the EIS detectors will sample all pitch angles. For lesser cone angles ($\Gamma = 65^{\circ} - 70^{\circ}$) rather complete pitch angle coverage is still obtained because of the finite opening angle of the detector system. For cone angles below $\sim 50^{\circ}$, pitch angles near 0° do not fall within the detector aperture at all. Regions where cone-angle effects are important will be pointed out when observations are presented.

DEFINITION OF THE DATA SET

The data used in this study were drawn from three experiments aboard IMP-8. The principle data were those obtained with the Caltech EIS as described in the previous section. Also used were magnetic field data and plasma data.

The magnetic field data covering the period from March to October 1974 were obtained with the Goddard Space Flight Center fluxgate magnetometer (R. P. Lepping and N. F. Ness, private communication, 1976). Magnetic field

vectors averaged over 15.36 seconds were provided in solar ecliptic and solar magnetospheric coordinate frames. Longer temporal averages of these basic vectors were calculated when appropriate.

The plasma data were obtained from the University of Iowa LEPEDEA experiment on IMP-8 (L.A. Frank, private communication, 1975). These data are summarized in the now familiar form of color-coded energy-time (E-t) spectrograms (see Frank and Ackerson, 1971 and Frank et al. 1976). Each spectrogram summarizes one twenty-four hour period with directional, differential intensity information provided separately for protons and electrons in the energy range 50 eV $\leq$ E $\leq$ 45 keV. There were 335 spectrograms available for 1974.

It has been a goal of this study to compare flux enhancements of electrons E $\geqslant$ 200 keV as revealed by the EIS with plasma events as seen in the E-t spectrograms. As a somewhat flexible working definition of a plasma "event", therefore, we have adopted the following: A distinct, relatively detached region in the E-t spectrogram for electrons in which the differential LEPEDEA intensity rises to at least $\sim 10^3$ counts sec^{-1} for some energy above 100 eV. Since counting rates near 100 eV are usually $\leqslant 10^2$ sec^{-1} even in the typical plasma sheet environment, such intensity increases as qualify for the above "event" definition are interpreted as indicating significant plasma heating (cf. Frank et al. 1976). There were $\sim$ 175 identifiable plasma events in the 335 spectrograms examined in 1974. These events were observed on 21 of 30 IMP-8 magnetotail passes and their occurrence was distributed over 45 of the 335 days.

The highly energetic electrons (E $\geqslant$ 200 keV) measured with the Caltech experiment were seen to significantly exceed background intensities at some time on virtually every magnetotail pass. The initial survey of the

intensities was done in terms of one-hour counting rate averages. Although large flux variations may occur within a one-hour time span, the hourly averages provide a reliable index of general magnetotail activity.

In Figure 2, based on the hourly averages of count rates for electrons $E \geqslant 200$ keV, we have plotted the number of periods for which the intensity exceeded two selected flux thresholds during each magnetotail pass of 1974. The magnetotail pass number is reckoned as the ascending node number of the particular orbit from the time of launch. In the upper part of Figure 2 we show the number of periods for which j ($E \geqslant 200$ keV) exceeded 2 $(cm^2\text{-sec-sr})^{-1}$ and below this is shown the number of hours for which j ($E \geqslant 200$ keV exceeded 10 $(cm^2\text{-sec-sr})^{-1}$.

A seasonal effect appears prominently in Figure 2 in that the duration of energetic electron detection is much longer for magnetotail passes occurring broadly near day 100 and day 270. Some 90 days before (or after) these periods, the duration of electron detection is typically $\leqslant 20\%$ as long. As several prior studies have shown, energetic electron fluxes associated with the plasma sheet are confined to regions within several R_E of the neutral sheet (see, eg., Montgomery el al. 1965, Bame et al. 1967, and Meng 1971). The lower panel of Figure 2 shows the spacecraft latitude, θ_{SM}, at the time that IMP-8 passed through the midnight meridian ($\phi_{SM} = 180^0$). This parameter gives a rough indication of proximity to the plasma sheet during a given magnetotail pass for the year of observation under discussion. From Figure 2 it is clear that the spacecraft's sampling of the magnetotail determines to a large extent the pattern of observations indicated in the upper panel of the figure.

Also indicated in Figure 2 are magnetotail passes during which there were extremely elevated electron rates due to solar activity. Although magne-

totail bursts were still often observed superimposed upon this solar background, we shall concentrate here on observations made during March-April of 1974, at which time solar electrons were not a factor.

OBSERVATIONS

The energetic electron events which form the basis of this report are conveniently studied according to the particular type of plasma region with which each is associated. Frank et al. (1976) have described magnetotail plasma phenomena and magnetic fields characteristic of three different domains: (1) the plasma sheet, (2) the boundary layer, which forms the transition region between the magnetotail and the magnetosheath (which is, furthermore, identified as the tailward extention of the polar cusp); and (3) the regions near, and within, the localized magnetotail acceleration regions (termed "fireball regions" by Frank et al.). In this paper we describe observations in the plasma sheet and in the fireball regions. In a companion paper we discuss our observations of the varied phenomenology of the boundary layer.

1. Plasma Sheet Events

As the first example of the magnetotail plasma sheet events at $\sim 30\ R_E$, we describe a period in which the EIS recorded a relatively high intensity of electrons $E \geqslant 200$ keV. This period occurred on 24 March (day 83) 1974. We show 4.1 minute averages of the quantities of interest in Figure 3. The basic format of Figure 3 is such that the abscissa is the universal time (UT) of data acquisition. In addition, at the bottom of the figure, spacecraft attitude information is provided at selected intervals. The information includes spacecraft latitude (θ_{SM}) and longitude (ϕ_{SM}), both in geocentric solar magnetospheric (GSM) coordinates, as well as geocentric radial distance

in earth radii (1 R_E = 6375 km). The spacecraft is seen to be slightly below the solar magnetospheric equator for the period shown in Figure 3 and is seen to be in the post-midnight longitude sector at ~ 33 R_E.

Magnetic field data are shown plotted in solar magnetospheric coordinates in the lowest three panels of Figure 3. Included are the total average field strength, F, measured in gammas (1 gamma = 10^{-5} gauss), the SM field azimuth, ϕ_B, and the Z component of the magnetic field, B_Z, also measured in gammas. The field strength varies between ~ 5 and ~ 20 gammas and the lowest field strengths are associated with four well-defined changes of ϕ_B by ~ 180° between ~ 0940 and ~ 1030 UT. Such field reversals along with small F values indicate examples of classic "neutral sheet" crossings. The Z-component of the magnetic field is zero or positive for virtually all of the day. There is an indication of slightly negative B_Z between 1100 and 1130 UT.

The absolute intensities of electrons E ⩾ 200 keV and E ⩾ 1 MeV are shown in the uppermost panel of Figure 3. The background levels for both the E ⩾ 200 keV and the E ⩾ 1 MeV channels are also indicated. These levels represent the typical portion of the counting rate subtracted as background from D0* and D01*, respectively, divided by the geometric factors of Table 1. Thus when the flux plotted for E ⩾ 200 keV approaches ~ 7 x 10^{-2} (cm^2-sec-sr)$^{-1}$ or when the flux plotted for E ⩾ 1 MeV approaches 1.2 x 10^{-2} (cm^2-sec-sr)$^{-1}$, the background correction is comparable to the measured flux.

Several electron flux enhancements are indicated by the EIS data and intensities of electrons E ⩾ 200 keV typical of the plasma sheet at 30 R_E (~10^1 cm^{-2} sec^{-1} sr^{-1}) are detected, for example, after 1330 UT. Note that the highest intensity of electrons E ⩾ 1 MeV (by about a factor of five) during this period occurs between ~ 0930 and ~ 1030 UT, i.e., at the time

of the neutral sheet crossings identified in the magnetic field data. Such an observation suggests similarities to the findings of Murayama and Simpson (1968), and Retzler and Simpson (1969) who observed relativistic electrons strongly correlated with the neutral sheet at ~ 19 and $\sim 38\ R_E$.

Primary attention is drawn, however, to the very large intensity enhancement in the $E \geqslant 200$ keV electrons between ~ 1200 and 1300 UT. A "flat-topped" intensity peak corresponding to j ($E \geqslant 200$ keV) $\sim 2 \times 10^3$ electrons $(cm^2\text{-sec-sr})^{-1}$ is reached between 1225 and 1255 UT. Moreover, this event is found to occur in association with an intense plasma heating event (L. A. Frank, private communication, 1975). Specifically, during the time period after 1200 UT, the average proton and electron energies more than double and the $E > 45$ keV electron intensities increase several orders of magnitude, but bulk plasma flows remain moderate ($\leqslant 400$ km sec^{-1}) throughout.

The second panel from the top of Figure 3 summarizes one method of investigating the spectral variation observed for this period. A differential energy spectrum obeying a power law in kinetic energy is assumed for the observed electrons and the ratio of the background-corrected count rates (DO1*/DO*) is then used to infer the value of γ in $\frac{dj}{dE} \propto E^{-\gamma}$. It is found that energetic electrons in the plasma sheet at 30 R_E are ordinarily distributed, using the present method, such that $2 \leqslant \gamma \leqslant 5$ (cf. periods following 1330 UT in Figure 3). In contrast, however, during the primary intensity enhancement between 1225 and 1255 UT of day 83, the computed spectral index increases substantially and lies in the range $6 \leqslant \gamma \leqslant 7$. Hence, a pronounced steepening of the energy spectrum is indicated.

To assess the appropriateness of a power law description of the energy spectrum, we have studied the detailed EIS pulse-height analysis

data. Resulting electron differential energy spectra for a sampling of periods preceding and during the main intensity enhancement on 24 March are shown in Figure 4. As discussed in the Instrumentation section, we have found it most suitable to use single parameter analysis and restrict detailed spectral analysis to channel groupings generally corresponding to the range 160 keV $\leqslant E \leqslant$ 2 MeV. We have also subtracted from all data shown a gamma-ray-induced background spectrum which was established from a three-day average obtained during an extended quiet-time period in late 1973. The background spectrum ordinarily contributes < 1% of the counting rate in the lower energy intervals, but it often does contribute significantly (10-20%) for the energy intervals with $E \sim 1$ MeV. A detailed laboratory calibration response matrix has been determined for the EIS instrument and a matrix inversion technique is used to obtain the spectral points as shown in Figure 4. Included with each of the data points is an error bar indicating the 1 σ uncertainty associated with the flux in the particular energy interval plotted. The periods covered by the spectra in Figure 4 are shown by the shaded regions in the upper panel of Figure 3.

Inspection of the five spectra shown for the selected 15-minute intervals reveals that, generally speaking, power law forms do appear to fit the pulse-height data well. Included with each spectrum is a least-squares power law fit to the flux points. Comparing the values of γ derived in this least-squares fitting procedure to the values of γ plotted in Figure 3, it is seen that rather good agreement is obtained for the 0930, 1210, 1240, and 1310 UT examples. This agreement is interpreted as supporting our assumption of the applicability of a simple power law spectrum for most of the event period.

Note, however, that a substantial discrepancy exists for the 1155-1210 UT interval. The ratio DO1*/DO* implies $\gamma \sim 4.5$ for this period,

whereas the PHA data indicate that $\gamma = 5.9 \pm 0.1$. Inspection of the data appear to confirm the quality of the fit to the PHA data in Figure 4. To resolve this question we have studied spectra for shorter subintervals in this time period and have found that the spectrum has a distinct break at ~ 500 keV and is formed of a low-energy portion going as E^{-6} and a high-energy portion going as $E^{-2.7}$. This results in an anomalously high integral response for $E \geqslant 1$ MeV (i.e., in DO1*). Thus the ratio DO1*/DO* is large and predicts a harder spectrum.

It is our conclusion, therefore, that the energetic electrons in the range 160 keV to ~ 2 MeV are ordinarily distributed according to a power law in energy. For limited periods this is not true, and a two-part spectrum is observed with a distinct break at ~ 500 keV. This appears to be a feature seen more commonly in the boundary layer and fireball regions, and is under further investigation. Finally, as the exemplary spectrum for 1240-1255 UT demonstrates, the energetic electron spectra become very soft (with $\gamma > 7$) at the peak intensity periods.

We return once again to the further information contained in Figure 3. An extensive study of the angular distributions of the electrons $E \geqslant 200$ keV on 24 March has been made. The properties of these angular distributions in terms of the first and second order anisotropies are summarized in the third through sixth panels of the figure. A simple Fourier analysis has been performed for each 4.1-minute sample period. An analytic form has been assumed as follows:

$$C(\phi) = C_0 \left[1 + S \cos(\phi - \Delta_1) + K \cos 2(\phi - \Delta_2) \right] . \qquad (1)$$

Here C represents the number of counts obtained in the azimuthal (ϕ) direction, while C_0 is the ommidirectional, or spin-averaged, number of counts. The terms within the brackets represent the degree of directional inten-

sity modulation. The middle term in the brackets of Eq.(1) represents first-order modulation which we identify as unidirectional streaming of particles (ordinarily along magnetic field lines). The parameter Δ_1 is the phase angle (in the coordinate ϕ) at which the intensity is a maximum, while the parameter S represents the relative streaming amplitude. The final term in the brackets of Eq.(1) represents second order modulation. This may ordinarily be of the bidirectional variety (a field-aligned or "cigar" distribution) with equal maxima in intensity along the positive and negative B-field directions, or it may be the bimodal variety (i.e., a "pancake" distribution) with a maximum intensity perpendicular to the local field line and axisymmetric about this line. Once again, Δ_2 is the second-order modulation phase angle and K represents the relative modulation amplitude of the pancake or cigar distribution. For measurement of complete isotropy, there is no modulation so that the parameters S and K above are equal to zero and $C(\phi) = C_0$. Isotropic, bimodal, and bidirectional distributions all indicate a strong mirror point magnetic field geometry in order that such symmetric distributions be maintained. The pancake distribution, in particular, is associated with trapped, or pseudo-trapped, particle populations on closed field lines.

Least squares fits assuming the form of Eq. (1) are made to the eight-sector roll angle distributions assembled for each sample period and the parameters C_0, S, K, Δ_1 and Δ_2 are regularly computed on this basis. The phase angle Δ_2 is periodic on the interval 0° to 180°, and thus we compute Δ_2 modulo 180°. One sigma uncertainties are also computed in the fitting procedure for each parameter and these are indicated by the error bars in Figure 3. The uncertainties decrease with increasing number of events, permitting accurate determination of progressively smaller anisotropies.

We have subtracted the ecliptic-plane projected (azimuthal) direction of the magnetic field vector (ϕ_B) from the computed values of Δ_1 and Δ_2 discussed in the last paragraph. The motivation for this subtraction is that the magnetic field should organize the particle motions and well-defined streaming should be along the field line $(\Delta_1 - \phi_B) \sim 0^o$ or 180°, whereas well-defined second order modulation should be either parallel to B $(\Delta_2 - \phi_B \approx 0^o)$ for bidirectional modulation or should be perpendicular to B $(\Delta_2 - \phi_B \approx 90^o)$ for bimodal distributions. The quantities $(\Delta_1 - \phi_B)$ and $(\Delta_2 - \phi_B)$ are, therefore, plotted in Figure 3.

It is seen in the third panel that streaming is small (usually $S \leqslant 0.1$) throughout the period covered, especially during periods when the largest electron intensities are detected. The (small) first order modulation which is detected has a rather randomly distributed phase with respect to the magnetic field longitude (as seen in the fourth panel). A few samples with statistically significant streaming and small second-order anisotropy are present between 1115 and 1130 UT at which time it was noted that B_Z was negative.

The second-order modulation amplitude, K, is comparable to, and often larger than, the streaming index, S. Particularly before ~ 1100 UT and after ~ 1300 UT, there is persistent modulation with $(\Delta_2 - \phi_B) \sim 90^o$, indicating pancake distributions. Near isotropy is found during the primary enhancement between 1225 and 1255 UT, but the phase is well-defined with $(\Delta_2 - \phi_B) \sim 0^o$. Hence a mild field-aligned bidirectionality is observed during the flux maximum and this characteristic has been seen during several other intense events during peak flux periods.

Energetic electron events such as shown for day 83 are frequently

seen in the plasma sheet with IMP-8 (and these may be more or less intense). Increases in absolute intensities (by factors of 10^2 to 10^3) accompanied by dramatic softening of the energy spectra are typical of ~ 20 distinct events, for example, between day 70 and day 120 of 1974. In each case, the $E \geqslant 200$ keV electrons were associated with the 50 ev $\leqslant E \leqslant 45$ keV plasma events observed simultaneously. The energetic electron enhancements were typified, too, by their association with regular magnetic fields that had nearly continuously northward B_Z components. Ordinarily, the electrons $E \geqslant 200$ keV had the symmetric pitch angle distributions of a quasi-trapped electron population as seen above. We show another example of this type to underscore the general characteristics, and also to demonstrate some contrasting features.

Figure 5 summarizes data obtained from IMP-8 for a portion of April 6 (day 96), 1974 i.e., on the magnetotail pass following that shown in Figure 3. The spacecraft in this case was in a generally similar position to that described for the 24 March event.

The magnetic field data are shown in the bottom three panels of Figure 5. As in the previous period described, the field strength, F, varies between ~ 5 and 20 gammas and several field azimuth reversals are evident wherein ϕ_B changed by $\sim 180^o$. During several periods of time, notably between 0430 and 0600 UT, the field is nearly vertical with $B_Z \sim F$.

The absolute intensities of electrons $E \geqslant 200$ keV and $E \geqslant 1$ MeV are shown in the uppermost panel of the Figure 5. Several small flux enhancements are evident in the flux profiles. Intensities of electrons $E \geqslant$ 200 keV typical of the plasma sheet at $\sim 30\ R_E$ are detected before $\sim$ 0330 UT and after $\sim$ 0630 UT. However, beginning at $\sim$ 0345 UT the intensity of electrons $E \geqslant 200$ keV rises rapidly by over four orders of magnitude to $\sim 10^4$ electrons $(cm^2\text{-sec-sr})^{-1}$, while the intensity of electrons $E \geqslant 1$ MeV

rises by about one order of magnitude. This enhancement is centered on a neutral sheet crossing (see ϕ_B) and furthermore represents one of the highest intensities recorded with the EIS on any magnetotail pass.

The general shape and character of the flux profile in Figure 5 suggests similarities to the primary enhancement of day 83 shown in Figure 3. The second panel of Figure 5 shows that the analogy extends also to the energy spectrum of the electrons since the spectral ratio (D01*/D0*) implies $\gamma \geqslant 6.5$. In other enhancements on day 96, $2 \leqslant \gamma \leqslant 5$, which has been noted to be more typical of the plasma sheet.

Figure 6 shows several differential energy spectra for the period encompassing the primary intensity enhancement on 6 April. The spectra are derived from the EIS pulse-height analysis data in the same fashion as described for those shown in Figure 4. The period covered by each spectrum is shown as a shaded bar in the upper panel of Figure 5.

As with the data shown for 24 March, the differential intensities for 6 April appear to be generally well-described by a single power law in energy. The fits made in the least-squares sense to the flux points are shown by the solid lines drawn through the data. The slopes of the fits in Figure 6 are to be compared with the spectral indices computed from the ratio D01*/D0* in the second panel of Figure 5. Although the count rate ratio often varies considerably during a given fifteen-minute interval, the average values of γ obtained from D01*/D0* are consistent with and in good agreement with the PHA spectra. The examples shown for 0430-0445 and 0445-0500 UT demonstrate once again the significant steepening of the spectrum which occurs for these events.

Returning attention to Figure 5, it is seen in the third panel that streaming is small (usually $S \leqslant 0.1$) throughout the period covered, especially between 0400 and 0600 UT when the largest electron intensities are detected.

The residual modulation which is detected has no well-defined phase with respect to the magnetic field longitude (as seen in the fourth panel). A few sample periods have S significantly above 0.1 and these occur in regions of quite low flux.

In contrast, the second order modulation is larger for much of the time period in Figure 5. Before 0345 UT, the phase angle $(\Delta_2 - \phi_B)$ is widely scattered and no well-established pitch angle distribution pattern is discerned for this region. From 0345 to 0410 UT, $(\Delta_2 - \phi_B)$ is $\sim 90^o$ indicating a mildly pancake character to the pitch angle distribution. From 0410 to 0445 UT when the highest absolute intensities are seen to occur, the modulation amplitude is small ($K \leqslant 0.05$) indicating apparent isotropy. However, the phase angle $(\Delta_2 - \phi_B)$ is well established and is seen to be near 0° (save for two sample periods near 0440 UT). Having $(\Delta_2 - \phi_B) \sim 0^o$ indicates a bidirectional character to the distribution. At 0445 UT a much stronger modulation appears at the time that the intensities begin to decline but it remains of the bidirectional kind. After 0515 UT and throughout the further decay phase of the event, sometimes strong pancake distributions are detected.

The explicit character of the electron angular distributions are shown in Figure 7 where the number of counts per sector is plotted versus solar ecliptic longitude. The azimuthal direction of the magnetic field, ϕ_B, is indicated in each small box by the positive vertical arrow while $(\phi_B - 180^o)$ is shown by the negative vertical arrow. The time of each sample (UT) is also indicated in each case. The 1 σ uncertainties are shown by error bars when they exceed the size of the plotted points. Each sample represents $\sim$ 20 seconds of data.

The apparent near-isotropy of the fluxes prior to 0445 UT is evident in Figure 7. However, as the examples between 0415 and 0425 UT show, a

mildly bidirectional (cigar) character is present during the period of maximum intensity.

The third vertical panel shows the much stronger bidirectional modulation detected beginning at ~ 0445 UT. The abruptness of this change can be understood in part in terms of the cone angle (Γ) which the magnetic field makes with the spacecraft spin vector. (The nature of cone angle effects was discussed above in the Instrumentation section). In the lower left-hand corner of each sample distribution in Figure 7 we show the total average field strength, F, and in the lower right hand corner we show the value of B_Z(both in gammas). When $B_Z \sim F$, only pitch angles near $\alpha \sim 90^o$ are sampled and when $B_Z \sim 0$ then all pitch angles are sampled. The third panel of Figure 7 shows that from 0440 to 0445 UT the magnetic field is essentially vertical and pitch angle coverage is minimal. Beginning with the 0447 UT sample,considerably more complete coverage ($\Gamma \sim 45^o$) is obtained and at that time the true strength of the bidirectional modulation is revealed. For times when $B_Z = F$ it is not possible to say what the true pitch angle distribution is. It is clear, however, that the true modulation amplitude is much larger after ~ 0445 UT than at ~ 0415 UT, for example.

The fourth panel of Figure 7 shows the change to pancake distributions observed beginning at ~ 0515 UT. Again cone angle effects play a role in determining the relative strength of the modulation; however, for a pancake distribution the maximum intensity (at $\alpha = 90^o$) is always correctly determined, even though the minimum intensity (at $\alpha = 0^o$) is not sampled.

For the event periods on 24 March and 6 April, the observed symmetric angular distributions indicate a closed field line structure. Con-

current plasma observations, Frank et al.(1976) show intense plasma heating for the day 96 event with more than a three-fold increase in average electron energy between 0300 and 0430 UT, for example. The intensities of electrons $E > 45$ keV increase dramatically at about 0400 UT, much as do the $E \geqslant 200$ keV electrons. Frank et al., however, find that the plasma bulk flow velocities remain small to moderate in magnitude with speeds in the range 50 to 500 km $(sec)^{-1}$. The flow is well ordered and generally antisunward for the entire period covered in Figure 5.

The bulk flow character combined with the continually northward B_Z component of the magnetic field (see Figures 3 and 5) have been suggested by Frank et al. (1976) as evidence that in the class of events described above we observe hot plasma and energetic particles injected onto the closed field lines of the plasma sheet. The detailed analysis performed for electrons $E \geqslant 200$ keV indicates angular distributions which are entirely consistent with this picture of confinement.

2. Fireball Encounter

On occasion the EIS detects energetic electron populations in the magnetotail which have properties that are in distinct contrast to those typical of the plasma sheet as discussed above. An example of such a period is shown in Figure 8. These data were obtained on 18 April (day 108) 1974. For the period shown, the spacecraft was located at a longitude $\phi_{SM} \geqslant 180^{o}$ at $\sim 32\ R_E$ geocentric distance. During this time the spacecraft remained between 3 and 6° above the GSM equatorial plane. The data from this period formed the basis of a prior brief report (Baker and Stone, 1976).

The magnetic field data are shown in the three lower panels of Figure 8. The directions of the magnetic fields as indicated by ϕ_B and B_Z, are notably variable and irregular between 0900 and 1400 UT. The field magnitude, F, is also very nonuniform and ranges from 3 to 25 gammas. Conditions of particular note in the plasma sheet magnetic field data, morever, are the extended periods of negative, or southward, B_Z (Frank et al. 1976). The primary regions where this field characteristic is seen are near 1100 UT and between 1300 and 1400 UT. Following ~1400 UT the field directions become much more regular in character again (similar to the fields seen on 24 March, for example, in Figure 3) and B_Z remains northward. Near 1700 UT typical neutral sheet crossings are seen in the magnetic fields.

The electron intensities $E \geqslant 200$ keV and $E \geqslant 1$ MeV are shown in the upper panel of Figure 8. The electron flux is not unusually large during this period, but the $E \geqslant 200$ keV intensity is quite variable. The electron flux $E \geqslant 1$ MeV remains relatively constant, on average, throughout the period at several times the background level.

Frank et al. (1976) have shown that during the period 0900 to 1400 UT shown in Figure 8, the plasma flow speeds were often remarkably large, at times exceeding 1000 km sec^{-1}. Moreover, these authors have found a one-to-one correlation of strong tailward velocities with negative B_Z and of strong earthward plasma jetting with positive B_Z. This contrasts considerably with the findings of Frank et al. in typical plasma sheet events.

Previous work (Baker and Stone, 1976; Frank et al. 1976) has also shown that the energetic electrons in this region have much different pitch angle distributions from those ordinarily witnessed in the plasma

sheet. In the third and fourth panels of Figure 8 we show the first and second-order modulation amplitudes, respectively, of electrons $E \geqslant 200$ keV as averaged over 4.1 minute intervals. During most periods of large fluxes ($\geqslant 10$ $(cm^2\text{-sec-sr})^{-1}$), both S and K are small (< 0.1). When fluxes of electrons $E \geqslant 200$ keV are ~ 1 $(cm^2\text{-sec-sr})^{-1}$, the S and K parameters have large error bars. It is seen that S and K are usually of comparable magnitude during low flux periods and are often consistent with zero. However, near 1100 UT and between $\sim$ 1300 and 1400 UT, S is often sizeable and is statistically well-determined. These periods correspond to times when B_Z is largely southward.

Better temporal resolution is useful to study the occurrence of energetic electron streaming. Figure 9 is similar to a figure shown by Baker and Stone (1976). It is analogous to Figure 7 and employs $\sim$ 20 second temporal resolution of the sectored EIS counting rates.

The first and fifth panels are sequences of distributions taken during flux enhancements when B_Z was continuously northward (the B_Z value in gammas is shown with each sample of Figure 9). In these series, i. e., near 1000 and 1630 UT, the electron fluxes are nearly isotropic. On the other hand, near 1100 UT and 1300 UT, at times when B_Z is southward, the second, third, and fourth panels of Figure 9 show that moderate to strong tailward streaming of the $E \geqslant 200$ keV electrons is often detected. Such distributions are possible only in the absence of a mirror geometry, as is expected for open field lines. Further inspection of the individual distributions shows that tailward streaming is present for magnetic field azimuths of both $\phi_B \sim 0^o$ and

$\phi_B \sim 180^o$. Thus strong net flow of 200 keV electrons is tailward on field lines characteristic of both the northern and southern halves of the magnetotail. Frank et al. (1976) have also reported detection of 10:1 tailward streaming of electrons E > 45 keV near 1100 UT of this day.

We note that the Z component of the magnetic field has substantial magnitude (both positive and negative) but B_Z is usually small enough compared to F that cone angle effects are not dominant. Hence, reasonably complete pitch angle coverage is usually obtained in this region.

As argued by Baker and Stone (1976) and Frank et al. (1976), observations such as the present ones of strong unidirectional streaming of energetic electrons on field lines with southward B_Z are strongly suggestive evidence that the field lines lack mirror geometry and are thus open to the interplanetary medium. The observation of extremely strong tailward jetting of plasma when B_Z is negative and corresponding strong earthward jetting when B_Z is positive has been used by Frank et al. (1976) to argue that this period on 18 April is a chance close encounter with the primary magnetotail acceleration region. In such regions there may be rapid dissipation of magnetic flux -- magnetic field line merging--at an X-type neutral point with concommitant intense plasma heating and energetic particle production. In this model one expects that tailward of the acceleration site (termed the magnetotail "fireball") merged field lines are open and have negative B_Z, while earthward of the fireball field lines are closed and have positive B_Z. The energetic electron angular distributions are consistent with this picture.

There are also distinguishing characteristics in the energy spectrum of the electrons observed in this region. The value of the spectral index inferred from the ratio DO1*/DO* (see the second panel of Figure 8) remains $\leqslant 5.5$ throughout the period shown. The value of γ drops, on occasion, to ~ 2 in the minimum intensity regions. However, it is useful to check the appropriateness of the power-law assumption made in Figure 8. In Figure 10 are shown several differential electron energy spectra derived from the EIS pulse height analysis data taken between $\sim$ 1000 and 1700 UT. The time interval over which each spectrum is taken is indicated by the shaded bars near the flux profiles in Figure 8.

Each of the PHA spectra taken between 1010 and 1140 UT (shown in Figure 10a) shows that a single power law is not a particularly good fit to the data. Each of the spectra appears to have a break in it between $\sim$ 500 keV and $\sim$ 1 MeV. In the 1010 and 1040 UT examples we have shown the least-squares fit to all the data points. In the 1055, 1110 and 1125 examples we show the fit to the differential intensities below 450 keV.

Comparing the PHA spectra of Figure 10a with the γ's of Figure 8, clearly indicates significant discrepancies between the spectral indices, Temporal variations may, of course, be responsible for some of the differences. Along with each PHA spectrum in Figure 10 we show the 15-minute average value of γ derived from DO1*/DO* and we define this as γ_*. In each example of Figure 10a, γ_* is much smaller than the fit to the pulse height data; this indicates a progressive hardening of the spectrum at higher energies (where the DO1* response lies).

The spectra shown in Figure 10b for 1240-1255, 1255-1310 and 1625-1640 UT are fit much better by a simple power law, as is also commonly the case in the typical plasma sheet environment. The γ_*'s and PHA indices agree well in

these examples also. We are devoting further study to this spectral character in the fireball regions (which has also been observed in boundary layer acceleration events).

For the magnetotail data studied most intensively to date, i.e., the 1974 IMP-8 data, one other region of the type described here (along with a possible third example) associated with close fireball encounters has been seen in the EIS magnetotail data. Brief, intense unidirectional streaming of electrons $E \geqslant 200$ keV occurred at $\sim$ 1900 UT on 8 October, 1974, when B_Z was southward and tailward plasma jetting was observed similar to the 18 April event (Frank et al. 1976).

SUMMARY OF OBSERVATIONS

Based on our survey of electrons $\geqslant 200$ keV detected with the Caltech EIS on IMP-8 during 1974, several conclusions may be drawn.

- Though no specific examples have been presented here, electrons $E \geqslant 200$ keV are observed beyond the bow shock of the earth, in the magnetosheath, and in the magnetotail boundary layer, as well as in the plasma sheet.
- The plasma sheet, as identified using the LEPEDEA plasma analyzers and the fluxgate magnetometer aboard IMP-8, is essentially continually populated with electrons $E \geqslant 200$ keV having intensities typically varying from near our flux threshold of $\sim 10^{-1}(\mathrm{cm}^2\text{-sec-sr})^{-1}$ to $\sim 10^2(\mathrm{cm}^2\text{-sec-sr})^{-1}$. A typical intensity would be $\sim 10\ (\mathrm{cm}^2\text{-sec-sr})^{-1}$.
- The typical plasma sheet electrons with energies between 160 keV and $\sim$ 2 MeV are seen by detailed pulse height spectral analysis to be distributed according to a simple power law in kinetic energy with spectral indices $2 \leqslant \gamma \leqslant 5$.

- As discussed extensively by Frank et al. (1976), B_Z is nearly continuously northward in the plasma sheet and we find this to be the case for the typical periods in which electrons $E \geqslant 200$ keV are present.
- Typical energetic electrons studied in the plasma sheet have angular distributions which are often consistent with isotropy.
- Clear electron enhancements $E \geqslant 1$ MeV are usually closely associated with neutral sheet crossings observed in the magnetic field data, whereas enhancements of electrons $E \geqslant 200$ keV are often not centered on neutral sheet crossings. However, close proximity to the neutral sheet is a prerequisite to the detection of large numbers of high intensity bursts $E \geqslant 200$ keV (cf. Figure 2).
- We recognize no pattern of streaming anisotropy of electrons $E \geqslant 200$ keV associated with neutral sheet crossings.
- Essentially all electron bursts $E \geqslant 200$ keV occurred in approximate coincidence with plasma events identified in the LEPEDEA E-t spectrograms (50 ev $\leq E \leq$ 45 keV).

For several magnetotail passes grouped around day 100 of 1974 and for several other magnetotail passes grouped around day 270, the IMP-8 orbit kept the spacecraft relatively near the magnetotail neutral sheet for substantial portions of the tail passage. During these orbits (occasionally several times per pass) energetic electron bursts with particularly high intensities were detected. In one class of such intense events, fluxes of 10^3 - 10^4 $(cm^2\text{-sec-sr})^{-1}$ were recorded.

- These very intense events regularly correlated with the most intense of the plasma heating events witnessed at lower energies (see discussion of Figures 3 and 5 above).

- These energetic electron bursts had extremely soft energy spectra, and detailed pulse height analysis showed them to be distributed as a power law in energy with spectral indices $\geqslant 6$.
- Throughout the course of the intense events, there was detection of statistically significant spin-modulation of the electrons $E \geqslant 200$ keV. First-order, or streaming, anisotropy amplitudes appeared generally negligible ($S \sim 0$) during the events, but second-order anisotropies were found to be persistently present. For the most intense portions of the events, anisotropy amplitudes were small ($K \leqslant 0.1$) often with a bidirectional (cigar) character. During the decay phase of the events both pancake and cigar distributions have been observed with $j_{max}/j_{min} \geqslant 2$.
- We note specifically that the Z component of the magnetic field was continually northward for these events (often strongly so) as was typically the case for the plasma sheet events of lesser magnitude.
- Frank et al. (1976) have shown the plasma bulk flows to remain moderate in speed for these events and have demonstrated that flow properties do not differ appreciably from other periods in the plasma sheet.

Occasionally within the magnetotail, moderately intense bursts of electrons $E \geqslant 200$ keV are observed which show markedly different behavior than is typical of the plasma sheet. These energetic electron bursts are found to be associated with the 'fireball' acceleration regions identified by Frank et al. (1976).

- Absolute intensities of electrons $E \geqslant 200$ keV reach levels which are rather high ($\geqslant 10^2$ $(cm^2\text{-sec-sr})^{-1}$), but not abnormally so. The intensities also appear extremely variable.

- Strong (> 10:1) unidirectional, field-aligned and tailward streaming is observed intermittently during the events. Absolute intensities often show substantial variations when streaming is detected, consistent with lack of magnetic confinement of the electrons.

- Tailward streaming is seen to be associated in some detail with regions of negative B_Z in the locally measured magnetic fields.

- Plasma (50 eV $\leq E \leq$ 45 keV) observations indicate strong earthward ($B_Z > 0$) and strong tailward ($B_Z < 0$) plasma jetting in these events (Frank et al., 1976).

- Energetic electrons show approximate isotropy when plasma jetting is earthward and streaming when plasma jetting is tailward.

- The detailed differential energy spectra for electrons $E \geqslant 160$ keV suggest a two-part spectrum with a break in the spectrum at $E \sim 500$ keV. This does not appear to be commonly observed in the typical plasma sheet flux enhancements.

DISCUSSION

The energetic electron characteristics seen most commonly in the current study (which we have therefore called typical) are similar to those reported in previous studies, many of which were made at lower energies. The instru-

mentation used in this work has offered a number of observational advantages over many previous studies including inherently low background, large geometric factors, excellent species identification, good angular distribution measurement capability, and availability of high resolution of differential intensities. Concurrent plasma and magnetic field data which were available in this study are indispensible for a complete picture of the complex phenomena in the magnetotail.

The intense electron bursts lasting tens of minutes to hours appear to have properties in significant contrast to the typical plasma sheet situation. These bursts are seen to have extremely soft spectra and have absolute intensities $E \gtrsim 200$ keV ranging up to $j \gtrsim 10^4 (cm^2\text{-sec-sr})^{-1}$. Although Sarris et al. (1976) observed similar bursts with IMP-7, they did not discuss in detail their observations of second-order anisotropies of electrons $E > 0.22$ MeV. We find substantial second-order anisotropies associated with the intense events. Strong second-order modulation of electron fluxes $E \geq 33$ keV was found by Singer and Bame (1970) and this was seen to occur almost exclusively near (inside) the magnetopause at $\sim 18\ R_E$. Singer and Bame interpreted their observed anisotropies as being of pancake character although they did not have magnetic field data available. The present observations (utilizing the locally-measured magnetic field direction) reveal that both pancake and cigar distributions are present for fluxes of electrons $E \gtrsim 200$ keV detected in the mid-tail region. Such observed electron distributions seem to provide clear evidence that the field lines threading the plasmas in the region of the spacecraft are closed.

Only in the fireball regions does the strong energetic electron streaming observed seem consistent with the open field lines expected in a field line

reconnection model. The variability of the intensities of electrons $E \geqslant 200$ keV also appears consistent with lack of confinement of the particles, i.e., with their relatively rapid escape from a source region past the spacecraft, probably into the interplanetary medium. The energy spectra observed during times of tailward streaming have a two-part character possibly consistent with two electron populations. We are studying this further to see if these spectra indicate active local acceleration to several hundred keV in energy combined with an ambient, relatively hard spectrum above ~ 500 keV. Our data currently suggests this may be so since the typical plasma sheet spectrum appears to be one continuous spectrum, i.e., that of a single electron population following a simple power law distribution. The very intense bursts also appear to be one electron population, but with a much softer spectrum.

A question of considerable importance is how electrons in the magnetotail are accelerated to hundreds of keV in energy. As the discussion of the fireball observations above indicated, the suggestion has been provisionally made that magnetic field-line merging is the ultimate energy source for the hot plasmas and energetic electrons in the magnetotail. This same basic mechanism has been postulated as an acceleration mechanism operating on the solar surface, in other planetary magnetospheres, and even in the interplanetary medium. In most of the forms in which the field-line merging mechanism is discussed, however, the potential differences postulated in the magnetotail models are of the order of tens of kilovolts but not hundreds or thousands of kilovolts. Consequently, the possibility that resonant wave-particle interactions produce the energization observed in the distant magnetotail should be considered.

Gurnett et al. (1976) have described the types of plasma waves observed with instrumentation on IMP-8 for the period under discussion in this study. Three types of noise are detected which include: 1) Broadband electrostatic emissions (10Hz - 1 kHz; 50 μV/m - 5mV/m) observed at the edges of the plasma sheet and in regions of large plasma bulk flows; 2) Whistler-mode magnetic noise bursts (10 - 300Hz;100 milligamma) observed near the neutral sheet and in regions with large magnetic field gradients near the edge of the plasma sheet i.e., generally in the same region as the largest broad-band electrostatic noise intensities; and 3) Narrow-band electrostatic emissions near harmonics of the electron gyrofrequency observed very infrequently by IMP-8 in the magnetotail.

Gurnett et al. (1976) have suggested that the broad-band electrostatic noise and the magnetic noise bursts may be produced by current driven instabilities or other sources of plasma free energy such as particle anisotropies. They have also pointed out the possibility that the observed plasma wave turbulence could be intense enough to produce the anomalous resistivity required in models of field line merging. On the other hand, it is suggested that the narrow-band electrostatic electron cyclotron emissions might be responsible for the acceleration of electrons to the energies ($E \geqslant 200$ keV) described in this study, through doppler-shifted cyclotron resonance interactions.

The broad-band electrostatic noise and the magnetic noise bursts are observed to be particularly intense in the heart of the fireball region, e.g., at ~ 1100 UT of 18 April, 1974. However, the electron cyclotron emissions are not detected at this particular time. Since the strong plasma jetting, plasma heating, and intense energetic electron streaming (along with atypical electron energy spectra) suggest active particle acceleration, specifically electron energization to several hundred kilovolts, it may be

that the broad-band electrostatic noise is resonantly interacting with the electrons to produce the observed acceleration.

The largest intensities of electrons $E \gtrsim 200$ keV which we observe with IMP-8 in the distant magnetotail have properties quite distinct from those in the fireball region. These intense events are associated with extremely hot plasmas on closed field lines. An example which we have discussed in detail, viz., the 6 April event, is precisely concurrent with the detection of intense narrow-band electron cyclotron emissions as reported by Gurnett et al. This suggests the possibility that the electron cyclotron waves, when present, also interact efficiently with the quasi-trapped electrons which are present on the closed field lines of the plasma sheet. Thus, these relatively rare cyclotron emissions may produce the atypically high-intensity, spectrally soft energetic electrons which have been described here. More detailed analysis of other events and modeling of the wave-particle interactions will help clarify the role of the plasma waves in the acceleration, redistribution in pitch angle, and loss processes of the very energetic electrons.

ACKNOWLEDGMENTS

We thank L.A. Frank both for providing us with the extensive set of IMP-8 LEPEDEA energy-time spectrograms used in this study prior to their publication and also for many halpful and informative discussions. We are grateful to R.P. Lepping and N.F. Ness for providing us with the IMP-8 magnetometer data through J.H. King of the National Space Science Data Center. We also thank R.E. Vogt who has been closely involved in this investigation and W.E. Althouse, G.J. Hurford, J.E. Lupton, and R.A. Mewaldt, who made significant contributions to various phases of this program. This work was supported in part by the National Aeronautics and Space Administration under contract NAS5-11066 and Grant NGR 05-002-160.

TABLE I. Electron response properties for the Caltech IMP-8 instrument (wide geometry)

DETECTION MODE[1]	Electron Detection Threshold	Collimator (Half-angle)	Effective Electron[2] Detection Energy	Effective Unidirectional[2] Geometric Factor
D0*	~ 0.16 MeV	$26^{\circ}.3$	$0.2 \leqslant E_e \leqslant 6$ MeV	1.6 ± 0.1 cm^2 -sr
D01*	~ 0.7 MeV	$24^{\circ}.4$	$1 \leqslant E_e \leqslant 6$ MeV	1.4 ± 0.1 cm^2 -sr

1 The designation D0* means electrons are counted in the front detector (labeled D0) and subsequently stop in the detector stack; D01* electrons are counted in coincidence by D0 and the second detector (D1) and subsequently stop in the detector stack.

2 The electron response functions rise gradually to peak efficiency above the threshold energy. The effective passbands and geometric factors are chosen to correspond to values least sensitive to spectral changes for a wide range of spectral forms.

REFERENCES

Anderson, K. A., Energetic electron fluxes in the tail of the geomagnetic field, J. Geophys. Res., 70, 4741, 1965.

Baker, D. N. and E. C. Stone, Energetic electron anisotropies in the magnetotail: Identification of open and closed field lines, Geophys. Res. Letters, 3, 557, 1976.

Bame, S. J., J. R. Asbridge, H. E. Felthauser, E. W. Hones, and I. B. Strong, Characteristics of the plasma sheet in the earth's magnetotail, J. Geophys. Res., 72, 113, 1967.

Frank, L. A. and K. L. Ackerson, Observations of charged particle precipitation in the auroral zone, J. Geophys. Res., 76, 3612, 1971.

Frank, L. A., K. L. Ackerson, and R. P. Lepping, On hot tenuous plasmas, fireball, and boundary layers in the earth's magnetotail, submitted to J. Geophys. Res., 1976.

Gurnett, D. A., L. A. Frank, and R. P. Lepping, Plasma waves in the distant magnetotail, submitted to J. Geophys. Res., 1976.

Haskell, G. P., Anisotropic fluxes of energetic particles in the outer magnetosphere, J. Geophys. Res., 74, 1740, 1969.

Hones, E. W., Jr., A. T. Y. Lui, S. J.Bame, and S. Singer, Prolonged tailward flow of plasma in the thinned plasma sheet observed at $r \approx 18\ R_E$ during substorms, J. Geophys. Res., 79, 1385, 1974.

Hurford, G. J., R. A. Mewaldt, E. C. Stone, and R. E. Vogt, The energy spectrum of 0.16 to 2 MeV electrons during solar quiet times, Astrophys. J., 192, 541, 1974.

Meng, C.-I., Energetic electrons in the magnetotail at 60 R_E, J. Geophys. Res., 76, 862, 1971.

Mewaldt, R. A., E. C. Stone, S. B. Vidor, and R. E. Vogt, Isotopic and elemental composition of the anomalous low energy cosmic ray fluxes, Astrophys. J., 205, 931, 1976.

Montgomery, M. D., S. Singer, I. P. Conner, and E. E. Stogsdill, Spatial distribution, energy spectra, and time variations of energetic electrons (E > 50 keV) at 17.7 earth radii, Phys. Rev. Letters, 14, 209, 1965.

Montgomery, M. D., Observations of electrons in the earth's magnetotail by Vela 2, J. Geophys. Res., 73, 871, 1968.

Murayama, T. and J. A. Simpson, Electrons within the neutral sheet of the magnetospheric tail, J. Geophys. Res., 73, 891, 1968.

Retzler, J., and J. A. Simpson, Relativistic electrons confined within the neutral sheet of the geomagnetic tail, J. Geophys. Res., 74, 2149, 1969.

Sarris, E. T., S. M.Krimigis, and T. P. Armstrong, Observations of magnetospheric bursts of high energy protons and electrons at $\sim 35\ R_E$ with IMP-7, J. Geophys. Res. 81, 2341, 1976.

Singer, S. and S. J. Bame, Anisotropic distributions of energetic electrons in the earth's magnetotail and magnetosheath, in Particles and Fields in the Magnetosphere, edited by B. M. McCormac, p. 122, D. Reidel, Dordrecht, Netherlands, 1970.

FIGURE CAPTIONS

Figure 1. A schematic illustration of the IMP-8 EIS. Detectors D0 through D10 are totally depleted surface-barrier solid-state detectors while D11 is a plastic scintillator anti-coincidence cup.

Figure 2. The upper panel shows the number of one-hour sample periods in which the IMP-8 EIS response to electrons $E \geqslant 200$ keV exceeded two selected flux thresholds during 1974. The horizontal shaded bars indicate magnetotail passes on which plasma events, as defined in the text, were observed. The lower panel shows the SM latitude of the spacecraft as it passed through the midnight median and, hence, provides a rough indication of the proximity to the neutral sheet during the year.

Figure 3. A summary of 4.1 minute averages of energetic electron fluxes (as labeled), energy spectral variations (γ), first- and second-order anisotropy amplitudes (S and K, respectively) and anisotropy phases relative to the magnetic field azimuth ($(\Delta_1 - \phi_B)$ and $(\Delta_2 - \phi_B)$, respectively) as detected with the EIS for a portion of 24 March, 1974. Magnetic field data (courtesy R. P. Lepping and N. F. Ness) shown in SM coordinates in the lower three panels include the total field strength (F, gammas), field azimuth (ϕ_B), and Z-component of the field (B_Z, gammas). At the bottom of the figure are shown the time UT of data acquisition plus the spacecraft latitude (Θ_{SM}), longitude (ϕ_{SM}), and geocentric radial distance (R_E).

Figure 4. Several differential energy spectra for electrons 160 keV $\leqslant$ E $\leqslant$ 2 MeV taken at the indicated times UT in the plasma sheet on 24 March 1974. The spectra are obtained from pulse-height analysis data as described in the text. The least-squares fits made to the flux points (assuming a power-law distribution in kinetic energy) are indicated by the solid line in each case.

Figure 5. A figure analogous to Figure 3 showing data obtained using IMP-8 for a portion of 6 April, 1974. See Figure 3 and text for description of plotted quantities.

Figure 6. Differential energy spectra for electrons as measured on 6 April, 1974 with the EIS. The data are analogous to those shown in Figure 4.

Figure 7. Several series of angular distributions of electrons E $\geqslant$ 200 keV observed for 6 April, 1974. The data plotted consist of the raw number of counts per sector versus solar ecliptic azimuth, ϕ_{SE}. Each distribution represents $\sim$ 20 seconds of data and 1 σ error bars are shown when they exceed the size of the plotted point. The magnetic field azimuth is shown by short vertical arrows for ϕ_B (+) and ϕ_B - 180° (-). Cone angle effects (see text) are important and with each sample we show the measured value of total magnetic field strength, F (lower left corner) and the value of B_Z (lower right corner). When $B_Z \sim$ F, incomplete pitch angle scans are obtained.

Figure 8. A summary of data obtained for a portion of 18 April, 1974 (cf. Figure 3). The period 0900 to 1400 UT has been identified by Frank et al. (1976) as a fireball encounter.

Figure 9. Angular distributions of electrons $E \geqslant 200$ keV observed on 18 April, 1974 (see Figure 7). Strong tailward, unidirectional streaming is observed intermittantly, usually associated with southward B_Z. The value of B_Z in gammas is indicated with each distribution.

Figure 10a. Detailed differential energy spectra for electrons in the fireball encounter region on 18 April, 1974. The data are analogous to those shown in Figures 4 and 6. For the 1010 -1025 and 1040-1055 spectra the least-squares fit is made to all flux points. For the 1055-1110, 1110 -1125 and 1125-1140 UT examples the fit is made for $E \leqslant 500$ keV. The spectral index γ_* shown with each example is the 15-minute average inferred from DO1*/DO* and indicates a pronounced hardening of the spectrum at high energies.

Figure 10b. Continuation of Figure 10a including a spectrum taken well-away from the tailward streaming (fireball) region, viz. the 1625-1640 UT example.

IMP-8
CALTECH ELECTRON/ISOTOPE SPECTROMETER

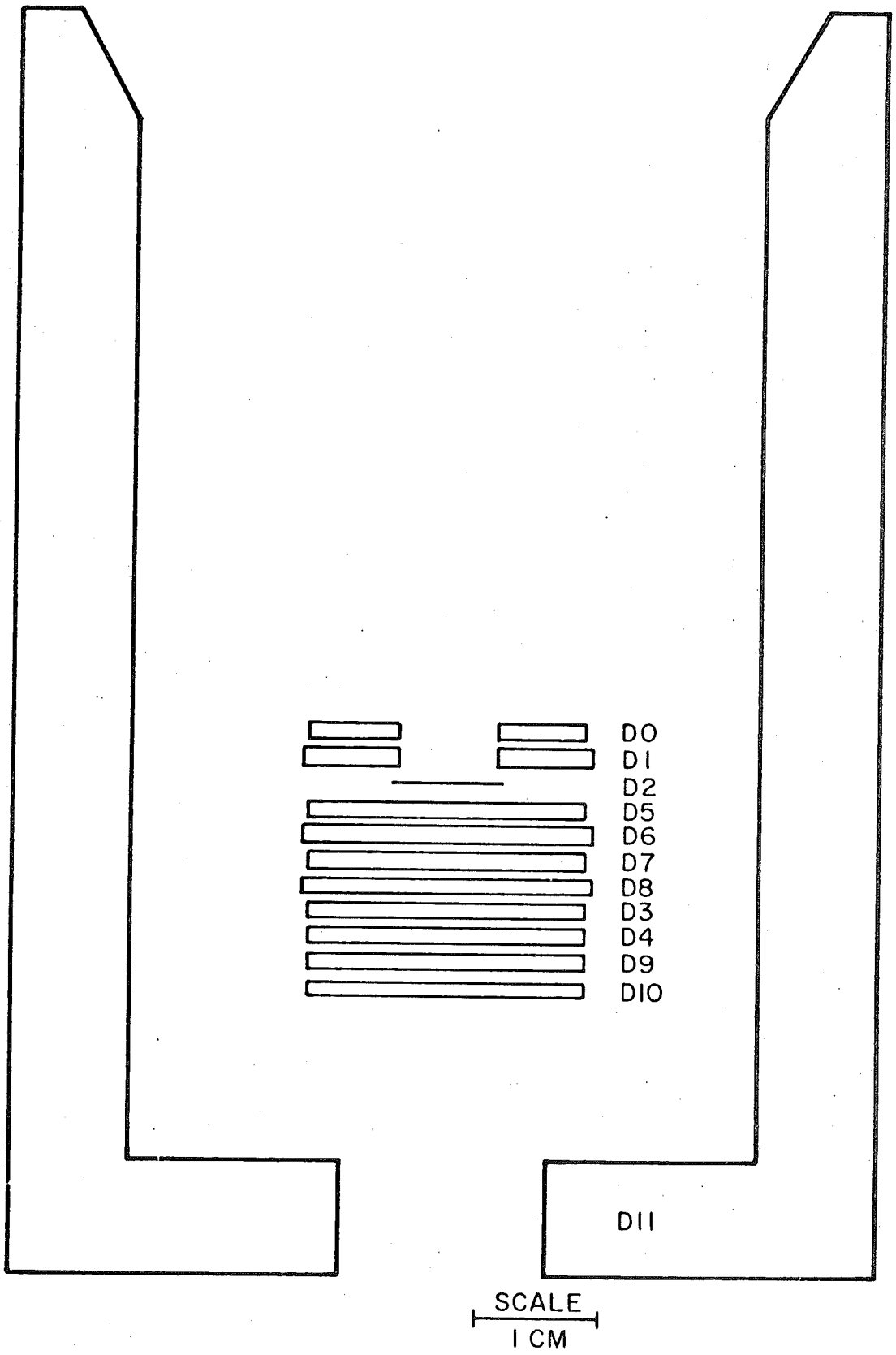

FIGURE 1

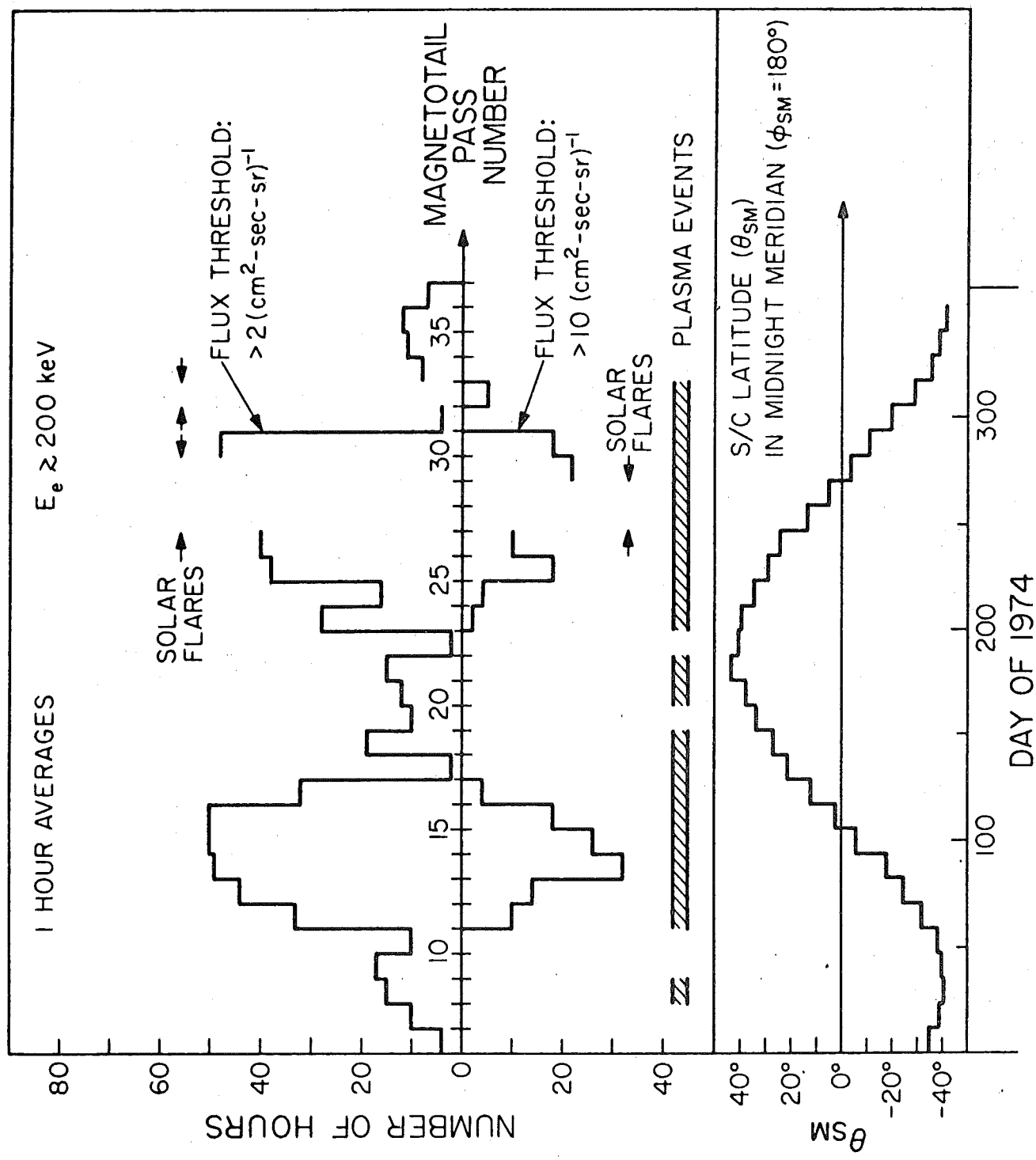
1 HOUR AVERAGES
$E_e \gtrsim 200$ keV
SOLAR FLARES
FLUX THRESHOLD: >2 (cm²-sec-sr)⁻¹
FLUX THRESHOLD: >10 (cm²-sec-sr)⁻¹
MAGNETOTAIL PASS NUMBER
SOLAR FLARES
PLASMA EVENTS
S/C LATITUDE (θ_{SM}) IN MIDNIGHT MERIDIAN (ϕ_{SM}=180°)
NUMBER OF HOURS
θ_{SM}
DAY OF 1974

FIGURE 2

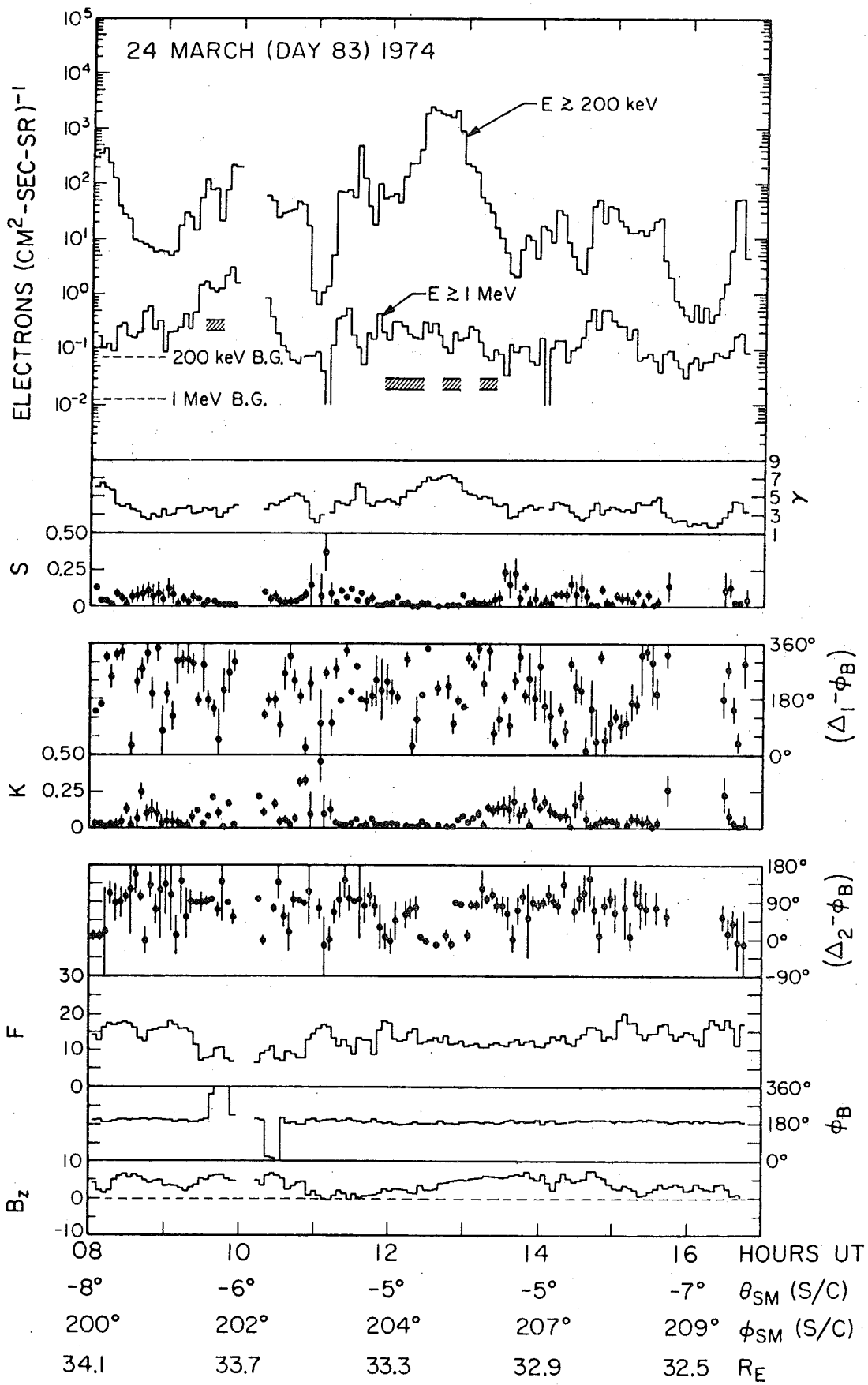
24 MARCH (DAY 83) 1974
ELECTRONS (CM²-SEC-SR)⁻¹
E ≳ 200 keV
E ≳ 1 MeV
200 keV B.G.
1 MeV B.G.
γ
S
K
(Δ1-φB)
(Δ2-φB)
F
φB
Bz
HOURS UT
θSM (S/C)
φSM (S/C)
RE

FIGURE 3

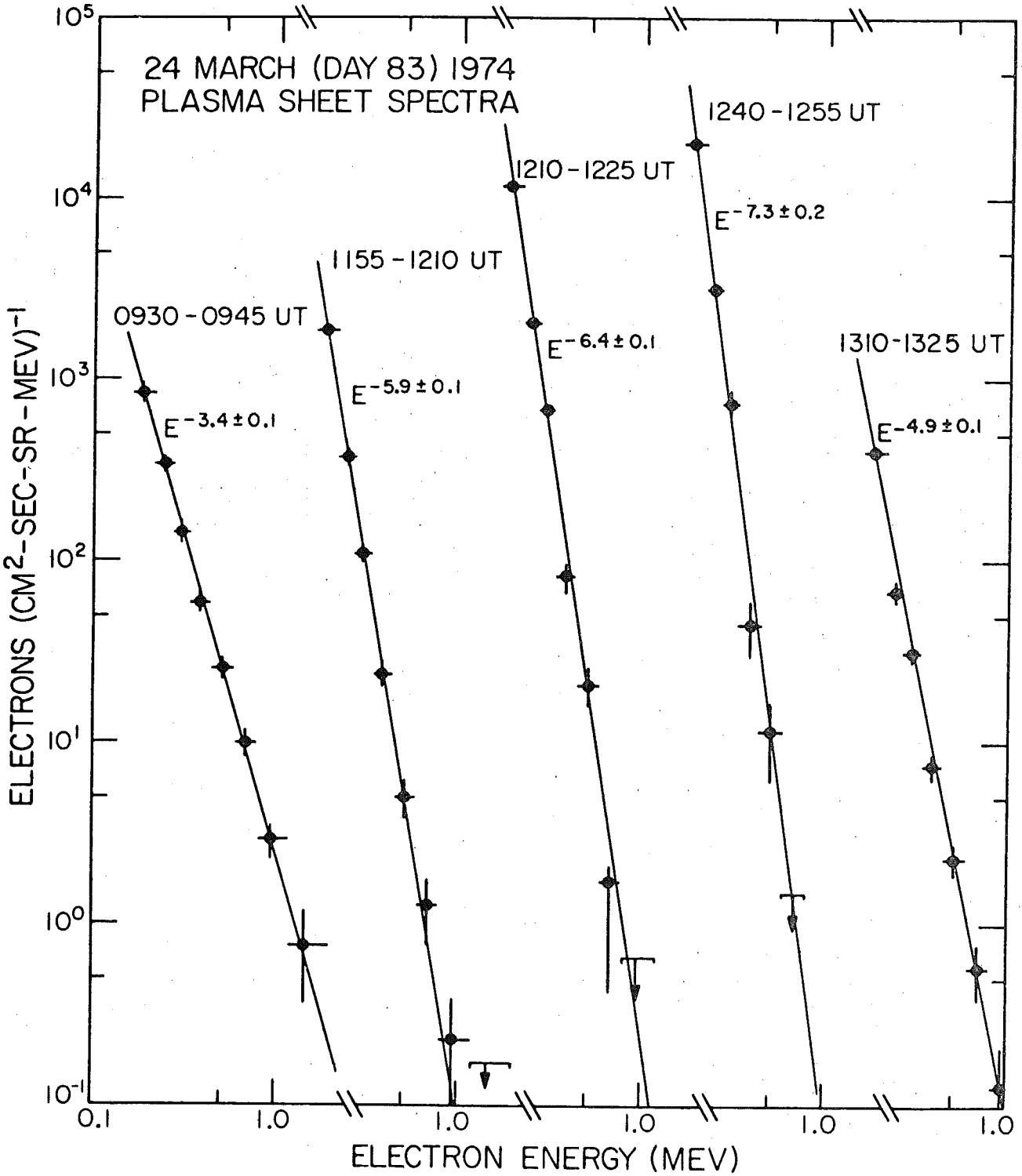
24 MARCH (DAY 83) 1974
PLASMA SHEET SPECTRA
0930 - 0945 UT
1155 - 1210 UT
1210 - 1225 UT
1240 - 1255 UT
1310 - 1325 UT
E^-3.4 ± 0.1
E^-5.9 ± 0.1
E^-6.4 ± 0.1
E^-7.3 ± 0.2
E^-4.9 ± 0.1
ELECTRONS (CM^2-SEC-SR-MEV)^-1
ELECTRON ENERGY (MEV)
10^5
10^4
10^3
10^2
10^1
10^0
10^-1
0.1
1.0
1.0
1.0
1.0
1.0

FIGURE 4

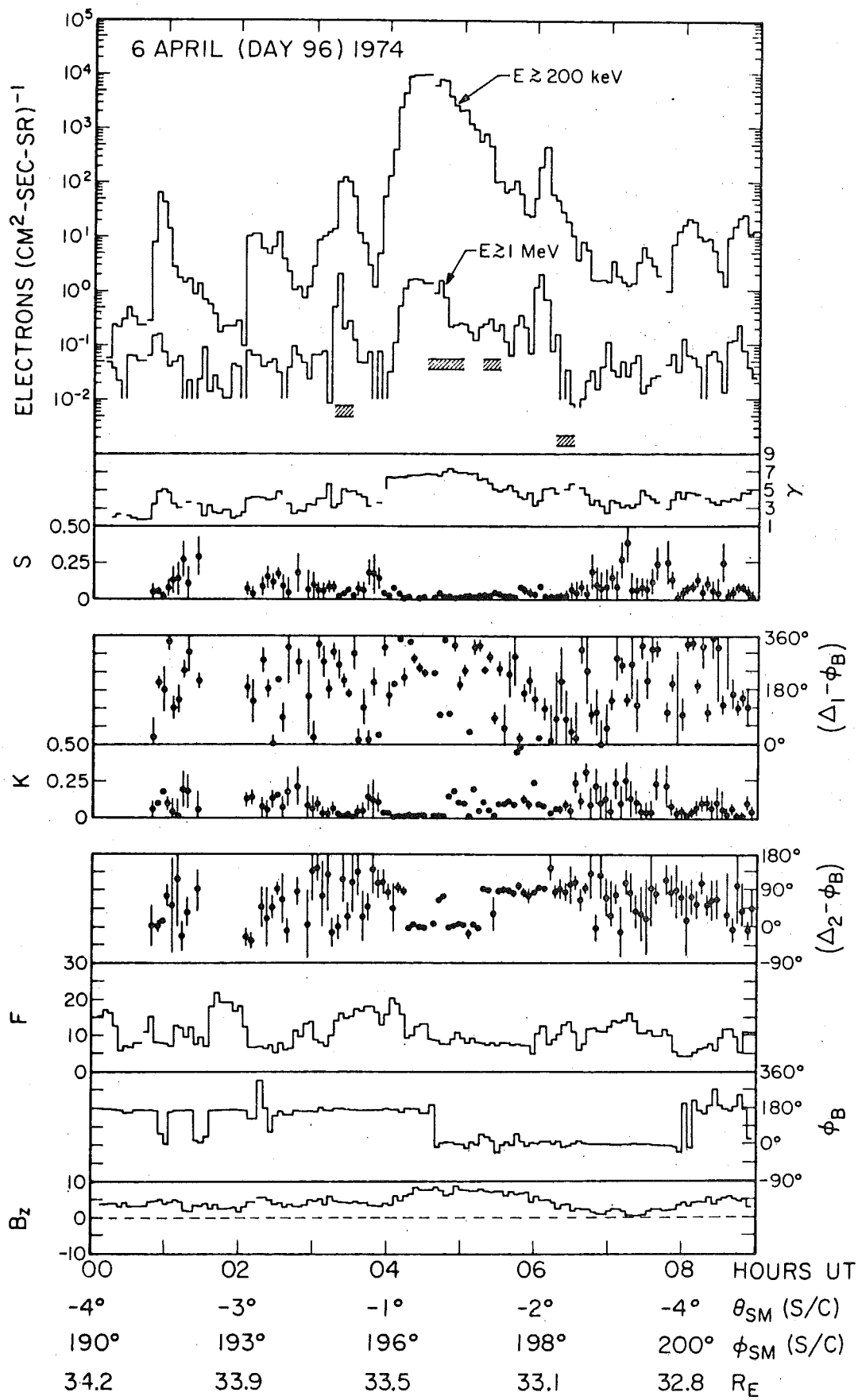
6 APRIL (DAY 96) 1974
E ≳ 200 keV
E ≳ 1 MeV
ELECTRONS (CM²-SEC-SR)⁻¹
γ
S
K
(Δ1 - φB)
(Δ2 - φB)
F
φB
Bz
HOURS UT
θSM (S/C)
φSM (S/C)
RE
00 02 04 06 08
-4° -3° -1° -2° -4°
190° 193° 196° 198° 200°
34.2 33.9 33.5 33.1 32.8

FIGURE 5

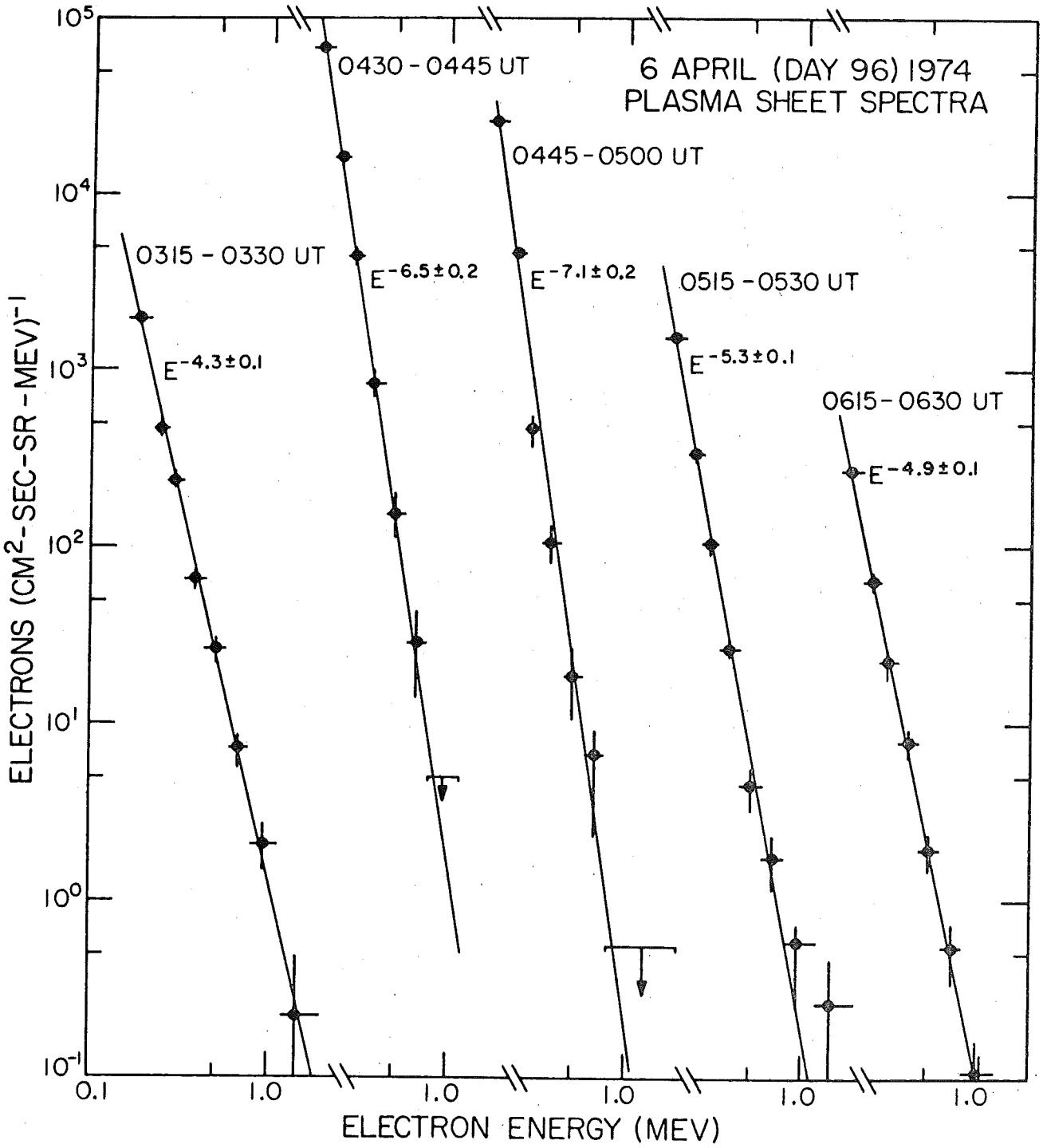
6 APRIL (DAY 96) 1974
PLASMA SHEET SPECTRA
0315 - 0330 UT
$E^{-4.3\pm0.1}$
0430 - 0445 UT
$E^{-6.5\pm0.2}$
0445 - 0500 UT
$E^{-7.1\pm0.2}$
0515 - 0530 UT
$E^{-5.3\pm0.1}$
0615 - 0630 UT
$E^{-4.9\pm0.1}$
ELECTRONS $(CM^2\text{-}SEC\text{-}SR\text{-}MEV)^{-1}$
10^5
10^4
10^3
10^2
10^1
10^0
10^{-1}
0.1
1.0
1.0
1.0
1.0
1.0
ELECTRON ENERGY (MEV)

FIGURE 6

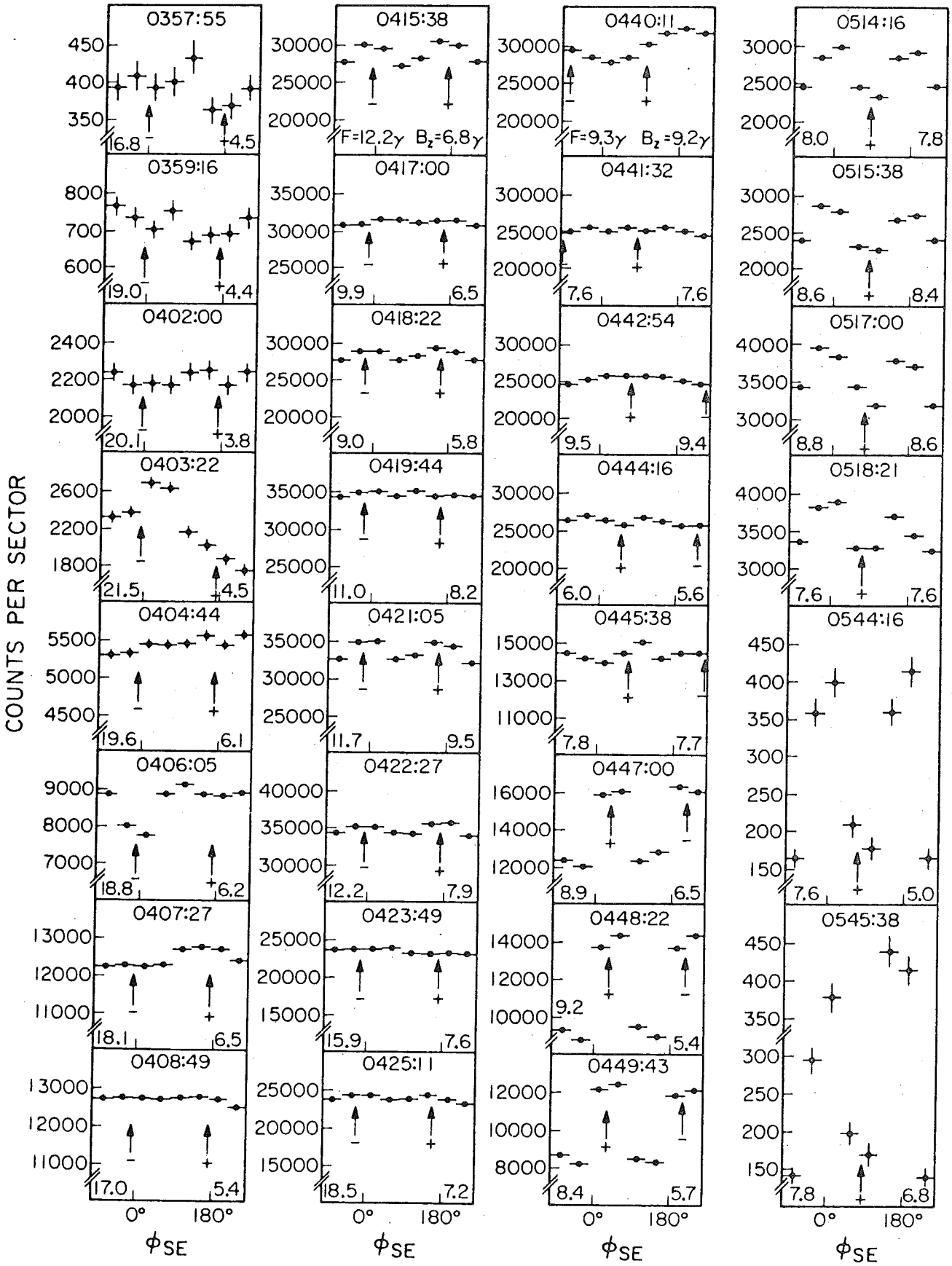
COUNTS PER SECTOR
0357:55
0359:16
0402:00
0403:22
0404:44
0406:05
0407:27
0408:49
0415:38
F=12.2γ B_z=6.8γ
0417:00
0418:22
0419:44
0421:05
0422:27
0423:49
0425:11
0440:11
F=9.3γ B_z=9.2γ
0441:32
0442:54
0444:16
0445:38
0447:00
0448:22
0449:43
0514:16
0515:38
0517:00
0518:21
0544:16
0545:38
0°
180°
φSE

FIGURE 7

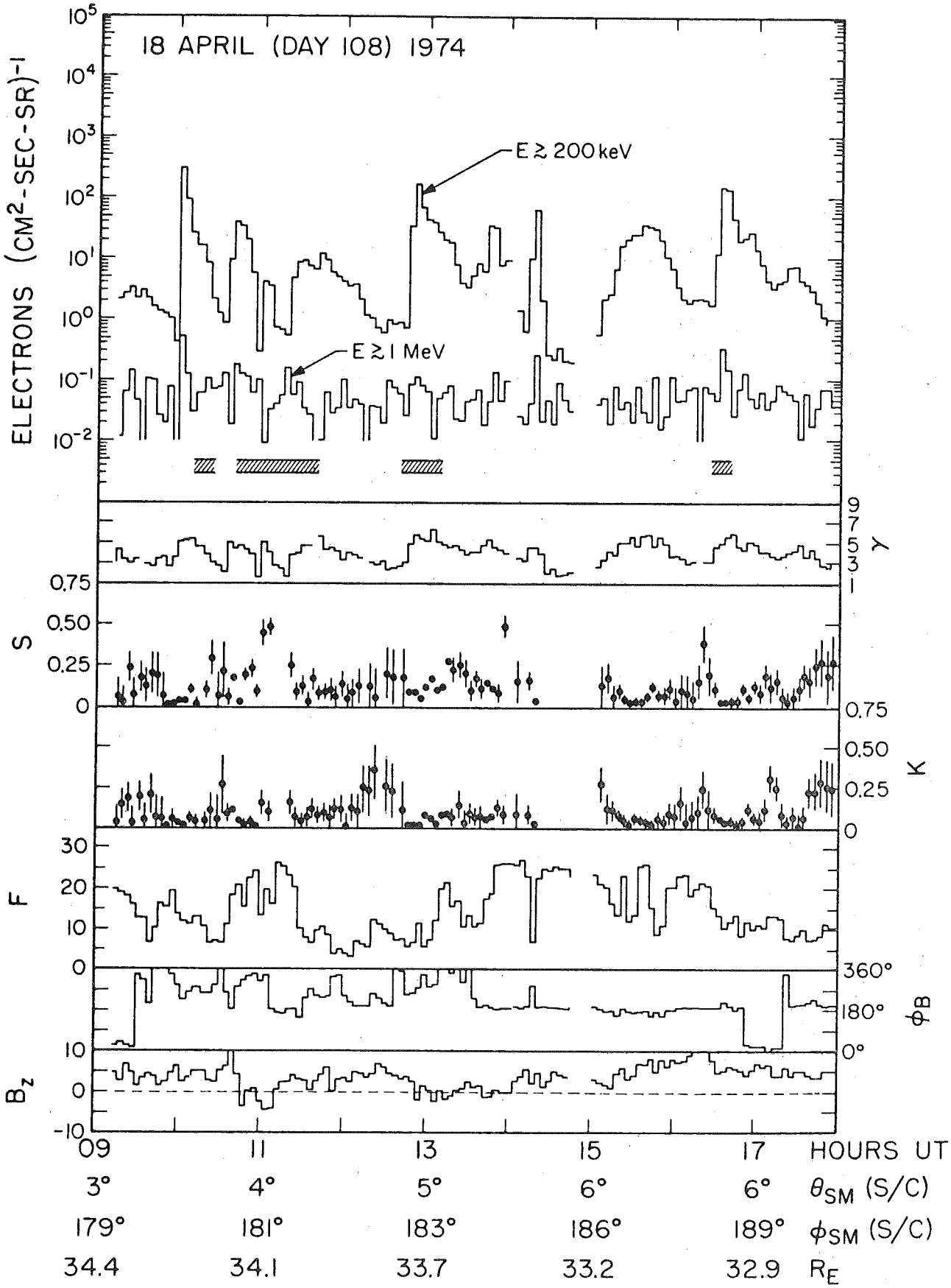
18 APRIL (DAY 108) 1974
ELECTRONS (CM²-SEC-SR)⁻¹
E ≳ 200 keV
E ≳ 1 MeV
γ
S
K
F
φB
Bz
HOURS UT
θSM (S/C)
φSM (S/C)
RE
09 11 13 15 17
3° 4° 5° 6° 6°
179° 181° 183° 186° 189°
34.4 34.1 33.7 33.2 32.9

FIGURE 8

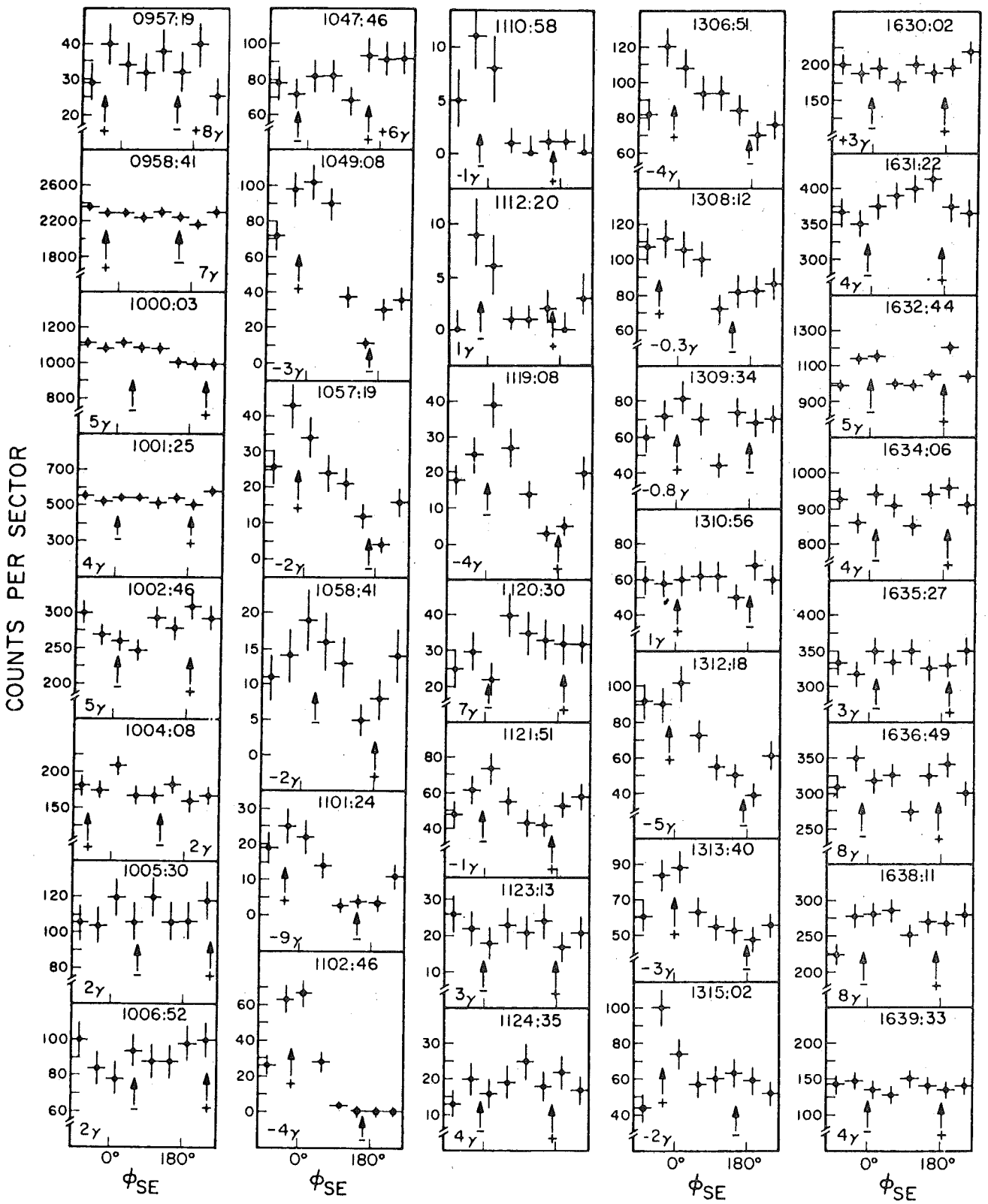
COUNTS PER SECTOR
0957:19
+8γ
0958:41
7γ
1000:03
5γ
1001:25
4γ
1002:46
5γ
1004:08
2γ
1005:30
2γ
1006:52
2γ
1047:46
+6γ
1049:08
-3γ
1057:19
-2γ
1058:41
-2γ
1101:24
-9γ
1102:46
-4γ
1110:58
-1γ
1112:20
1γ
1119:08
-4γ
1120:30
7γ
1121:51
-1γ
1123:13
3γ
1124:35
4γ
1306:51
-4γ
1308:12
-0.3γ
1309:34
-0.8γ
1310:56
1γ
1312:18
-5γ
1313:40
-3γ
1315:02
-2γ
1630:02
+3γ
1631:22
4γ
1632:44
5γ
1634:06
4γ
1635:27
3γ
1636:49
8γ
1638:11
8γ
1639:33
4γ
0°
180°
ϕ_{SE}

FIGURE 9

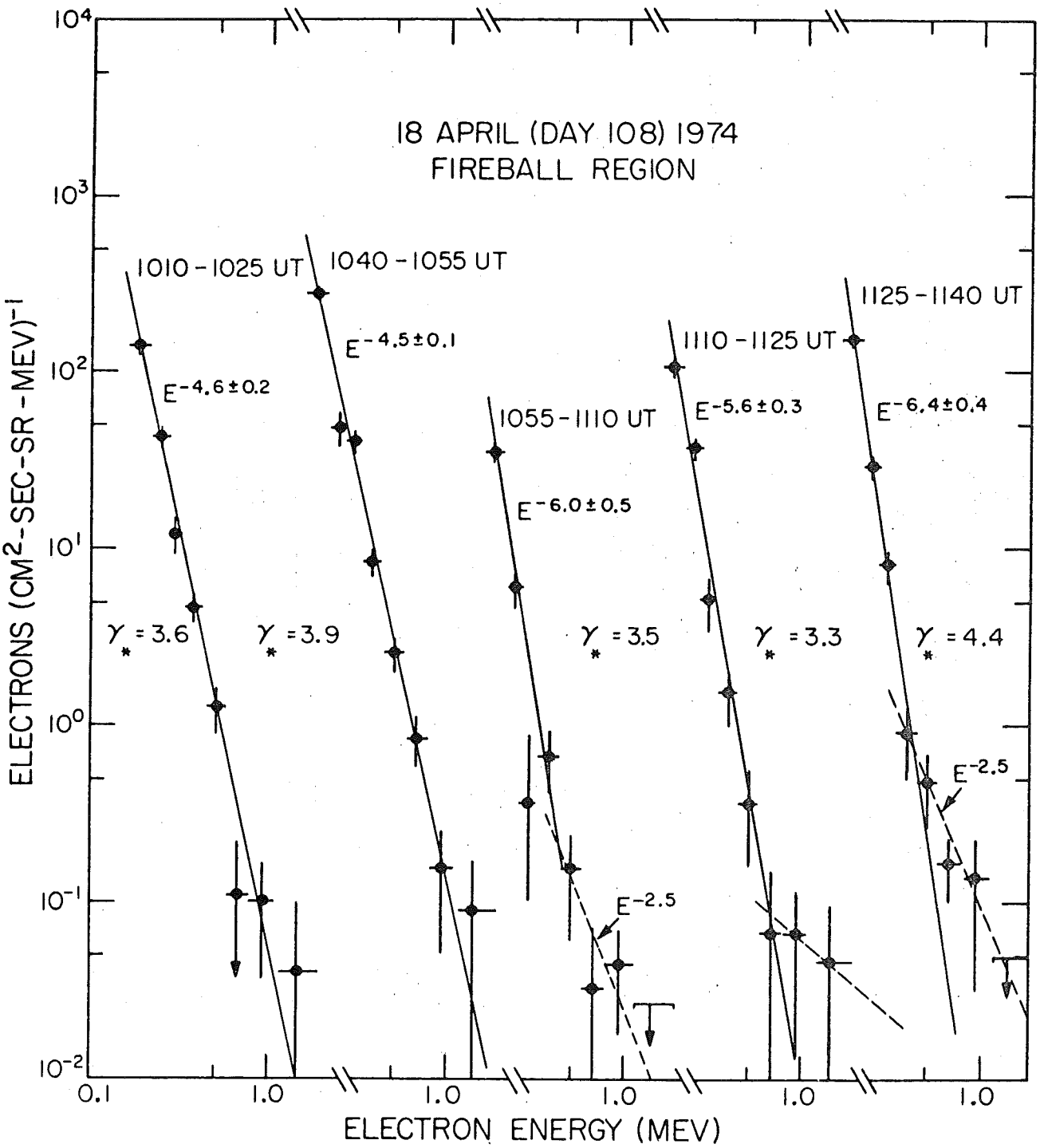
18 APRIL (DAY 108) 1974
FIREBALL REGION
1010 - 1025 UT
1040 - 1055 UT
1055 - 1110 UT
1110 - 1125 UT
1125 - 1140 UT
E^-4.6±0.2
E^-4.5±0.1
E^-6.0±0.5
E^-5.6±0.3
E^-6.4±0.4
γ* = 3.6
γ* = 3.9
γ* = 3.5
γ* = 3.3
γ* = 4.4
E^-2.5
E^-2.5
ELECTRONS (CM^2-SEC-SR-MEV)^-1
ELECTRON ENERGY (MEV)
10^4
10^3
10^2
10^1
10^0
10^-1
10^-2
0.1
1.0
1.0
1.0
1.0
1.0

FIGURE 10a

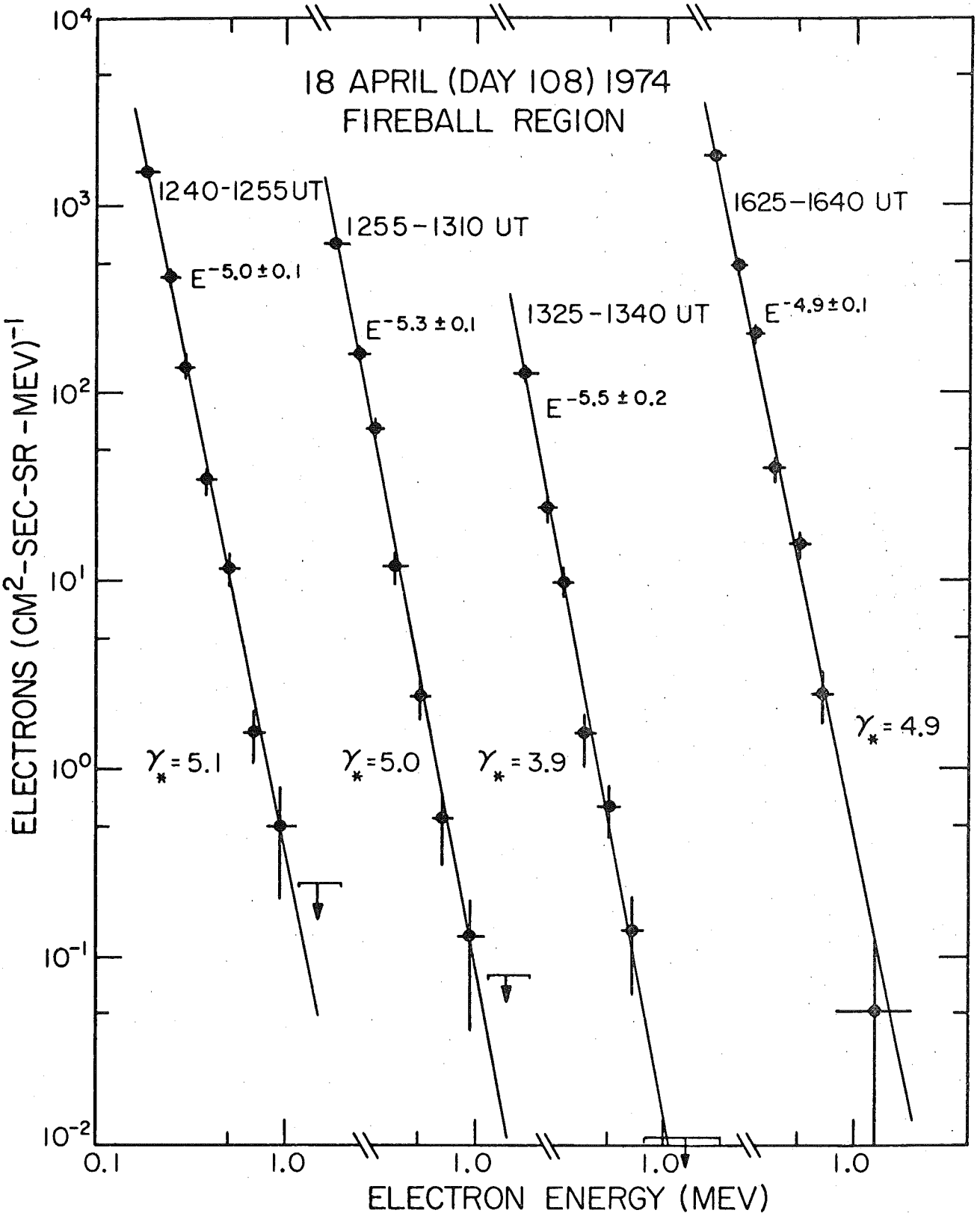
18 APRIL (DAY 108) 1974
FIREBALL REGION
1240-1255 UT
1255-1310 UT
1325-1340 UT
1625-1640 UT
$E^{-5.0 \pm 0.1}$
$E^{-5.3 \pm 0.1}$
$E^{-5.5 \pm 0.2}$
$E^{-4.9 \pm 0.1}$
$\gamma_* = 5.1$
$\gamma_* = 5.0$
$\gamma_* = 3.9$
$\gamma_* = 4.9$
ELECTRONS $(CM^2\text{-}SEC\text{-}SR\text{-}MEV)^{-1}$
10^4
10^3
10^2
10^1
10^0
10^{-1}
10^{-2}
0.1
1.0
1.0
1.0
1.0
ELECTRON ENERGY (MEV)

FIGURE 10b